ORIGINAL ARTICLE

Sedimentologic and stratigraphic criteria to distinguish between basin-floor and slope mudstones: Implications for the delivery of mud to deep-water environments

Kévin Boulesteix[1] | Miquel Poyatos-Moré[2] | Stephen S. Flint[1] | David M. Hodgson[3] | Kevin T. Taylor[1] | Rufus L. Brunt[1]

[1]Department of Earth and Environmental Sciences, University of Manchester, Manchester, UK

[2]Departament de Geologia, Universitat Autònoma de Barcelona, Cerdanyola del Vallés, Spain

[3]School of Earth and Environment, University of Leeds, Leeds, UK

Correspondence
Kévin Boulesteix, Department of Earth and Environmental Sciences, University of Manchester, Oxford Road, 10 Manchester M13 9PL, UK.
Email: kevin.boulesteix@gmail.com

Abstract

Deep-water mudstones overlying basin-floor and slope sandstone-prone deposits are often interpreted as hemipelagic drapes deposited during sand starvation periods. However, mud transport and depositional processes, and resulting facies and architecture of mudstones in deep-water environments, remain poorly understood. This study documents the sedimentology and stratigraphy of basin-floor and slope mudstones intercalated with sandstone-prone deposits of the Laingsburg depocentre (Karoo Basin, South Africa). Sedimentologic and stratigraphic criteria are presented here to distinguish between slope and basin-floor mudstones, which provide a tool to refine palaeogeographical reconstructions of other deep-water successions. Several mudstone units were mapped at outcrop for 2500 km^2 and investigated using macroscopic and microscopic core descriptions from two research boreholes. Basin-floor mudstones exhibit a repeated and predictable alternation of bedsets dominated by low-density turbidites, and massive packages dominated by debrites, with evidence of turbulent-to-laminar flow transformations. Slope mudstones exhibit a similar facies assemblage, but the proportion of low-density turbidites is higher, and no repeated or predictable facies organisation is recognised. The well-ordered and predictable facies organisation of basin-floor mudstones suggest local point sources from active slope conduits, responsible for deposition of compensationally stacked muddy lobes. The lack of predictable facies organisation in slope mudstones suggests deposition took place in a more variable range of sub-environments (i.e. ponded accommodation, minor gully/channel-fills, levees). However, regional mapping of three mudstone units evidence basinward tapering and similar thicknesses across depositional strike. This geometry is consistent with the distal part of basin margin clinothems, and suggests laterally extensive mud delivery across the shelf edge combined with along-margin transport processes. Therefore, the sedimentology and geometry of mudstones suggests that mud can be delivered to deep-water dominantly by

sediment gravity flows through point source and distributed regionally, during periods of up-dip sand storage. These findings challenge the common attribution of deep-water mudstones to periods of basin-floor sediment starvation.

KEYWORDS

basin-floor, depositional processes, Karoo Basin, mudstones, slope

1 | INTRODUCTION

The nature of sediment supplied from shelf to deep-water environments is controlled by a complex interplay between accommodation, basin margin physiography and process regime, tectonics and climate (Bourget et al., 2014; Carvajal & Steel, 2009; Cosgrove et al., 2018; Dixon et al., 2012; Gong et al., 2016; Hadler-Jacobsen et al., 2005; Laugier & Plink-Björklund, 2016; Paumard et al., 2020). Sand is preferentially delivered to deep-water environments when fluvio-deltaic systems are near to (or at) the shelf edge (Steel et al., 2003), when the shelf is exposed and incised (Johannessen & Steel, 2005; Porębski & Steel, 2003; Suter et al., 1987), and/or through shelf-incised canyons that capture longshore drift sediments (Covault et al., 2007). Sand can be delivered beyond the shelf edge through long-lived fixed submarine canyons (point source), or relatively uniformly over the shelf margin through multiple short-lived slope conduits or sheet-like flows (Gorsline, 1978; Reading & Richards, 1994), that is, line sourced. In the absence of significant sand transfer beyond the shelf edge, commonly during times of high shelf accommodation, the coeval deep-water deposits are fine grained, and interpreted as low-energy hemipelagic drapes (Flint et al., 2011; Posamentier & Kolla, 2003; Posamentier & Walker, 2006). Mud is deposited along the basin margin as laterally extensive units (Gervais et al., 2006; Pyles, 2008; Sweet et al., 2019; Sylvester et al., 2012; Van der Merwe et al., 2010; Wynn et al., 2000). Typically, these deposits are overlooked relative to their sandstone-prone counterparts, due to their fine-grained nature, and are commonly referred to as 'background' deposits.

Several studies have documented the transport and deposition of mud in ancient shelf environments (Macquaker & Gawthorpe, 1993; Schieber, 1994; Macquaker et al., 2007; Plint, 2014; Poyatos-Moré et al., 2016). Monitoring of modern shelf settings showed that large amounts of mud can be transported to the shelf edge and canyon heads by wave, storm or river activity, before being transferred downslope by sediment gravity flows (Bourrin et al., 2015; Palanques et al., 2006; Puig et al., 2003; Walsh & Nittrouer, 1999). These observations suggest that the transfer of mud from shelf to deep-water environments might be more energetic than previously envisaged. Even though Ocean Drilling Program (ODP) expeditions identified terrestrial organic

matter associated with turbidites in deep-ocean basins (Summerhayes, 1981; Tissot et al., 1980), only a few studies have focussed on the wide range of depositional processes recorded in deep-water mudstones (low-density turbidity currents, debris flows, transitional flows, bottom currents, hemipelagic settling) (Boulesteix et al., 2019, 2020; Emmings et al., 2020; Könitzer et al., 2014; Loucks & Ruppel, 2007; Newport et al., 2018; Schieber, 1999; Trabucho-Alexandre et al., 2011). However, these studies tend to focus on either slope or basin-floor deposits using one-dimensional datasets, and in general lack a well-constrained three-dimensional stratigraphic framework. No previous studies have sought to compare mud-dominated slope and basin-floor deposits in the same succession, and therefore, an investigation of the differences in depositional processes and facies stacking patterns between these deposits is necessary.

The aim of this study is to document the sedimentology and stratigraphy of several deep-water mudstone units, intercalated with sandstone-prone deposits, which encompass the basin-floor to slope transition, in the Laingsburg depocentre (Karoo Basin, South Africa). Through detailed core descriptions from two research boreholes, integrated with the three-dimensional stratigraphic control established by previous studies, the specific objectives are: (i) to understand the range of processes transporting and depositing mud in slope and basin-floor environments; (ii) to provide sedimentologic and stratigraphic criteria to differentiate basin-floor from slope mudstones; and (iii) to discuss the implications for the delivery and transport of mud to deep-water environments.

2 | GEOLOGICAL SETTING

The Karoo Basin of South Africa has been interpreted as a retroarc foreland basin that formed during the Carboniferous and Permian on the southern margin of Gondwana, with subsidence controlled by flexural loading linked to the development of a magmatic arc and associated fold–thrust belt (Cape Fold Belt) (Catuneanu et al., 1998; De Wit & Ransome, 1992; Veevers et al., 1994; Visser & Prackelt, 1996). More recent studies suggest that subsidence during the early deep-water pre-foreland basin phase was associated with dynamic topography (mantle

flow of Pysklywec & Mitrovica, 1999), with a later transition to a retroarc foreland basin stage during the Triassic (Blewett & Phillips, 2016; Tankard et al., 2009, 2012).

The Laingsburg depocentre, situated in the south-western Karoo Basin, is bounded to the south by the Swartberg Branch of the Cape Fold Belt (Figure 1A,B). The sedimentary fill comprises the Late Carboniferous to Early Jurassic Karoo Supergroup, subdivided into glacial deposits of the Dwyka Group (Late Carboniferous to Early Permian), the post-glacial clastic marine Ecca Group (Permian), and the continental Beaufort Group (Permian to Triassic) (Figure 1C) (Johnson et al., 1996; Smith, 1990). The Lower Ecca Group (350 m thick) comprises the Prince Albert, Whitehill and Collingham formations, deposited in a sand-starved basin-floor environment (Figure 1C) (Chukwuma & Bordy, 2016; Viljoen, 1994; Visser, 1992). The overlying Upper Ecca Group (1800 m thick) comprises: (i) distal basin-floor deposits of the Vischkuil Formation (Van der Merwe et al., 2009, 2010); (ii) basin-floor fans to base-of-slope deposits of the Laingsburg Formation (Units A, A/B, B) (Sixsmith et al., 2004); (iii) submarine slope channel-levee complexes and incised slope valley deposits of the Fort Brown Formation (Units B/C, C, D, D/E, E, F, G) (Di Celma et al., 2011; Hodgson et al., 2011); and (iv) shelf-edge and shelf deposits of the Waterford Formation (Jones et al., 2015; Poyatos-Moré et al., 2016) (Figure 1C,D).

2.1 | Laingsburg and Fort Brown formations

The architecture and depositional environments of the Laingsburg and Fort Brown formations are constrained by a robust three-dimensional stratigraphic framework, established through extensive mapping over 2500 km^2 (Figure 1B,D) (Brooks et al., 2018a; Brunt et al., 2013a, 2013b; Di Celma et al., 2011; Figueiredo et al., 2010; Flint et al., 2011; Grecula et al., 2003a, 2003b; Hodgson et al., 2011; Morris et al., 2016; Morris et al., 2014a, 2014b; Poyatos-Moré et al., 2019; Sixsmith et al., 2004; Spychala et al., 2015, 2017; Van der Merwe et al., 2009, 2010, 2014). Palaeoflow was dominantly to the north-east and east, and the main sediment entry point was located to the south-west (Van der Merwe et al., 2014). The coeval shelf deposits of the Laingsburg and Fort Brown formations are absent because of later uplift and erosion of the Cape Fold Belt. The stratigraphic framework of the Laingsburg (Units A, A/B, B) and Fort Brown (Units B/C, C, D, D/E, E, F, G) formations is based on the recognition and mapping of continuously exposed regional mudstone units intercalated between sandstone-prone units. Overall, mudstone units thin gradually basinward (to the east)

forming a wedge-shape geometry (Brooks et al., 2018a; Brunt et al., 2013b; Poyatos-Moré et al., 2019), and locally infill and heal residual depositional topography such as channel-fills and levees (Morris et al., 2016) (Figure 1D). The relative thicknesses of the mudstone units have been used as a tool to propose a hierarchical subdivision of the deep-water succession (Flint et al., 2011).

In a sequence stratigraphic framework, the Laingsburg and Fort Brown formations have been subdivided into four composite sequence sets, the first comprising Unit A, the second Units A/B and B, the third Units B/C, C and D and the fourth Units D/E, E and F (Flint et al., 2011). Each of these composite sequence sets can be subdivided into composite sequences, which can be further subdivided into sequences, where the sandstone-prone units have been interpreted as lowstand systems tracts, and the regional mudstone units as combined transgressive and highstand systems tracts (Flint et al., 2011). Here, the focus is on the sedimentology and stratigraphy of regional mudstone units deposited in basin-floor to base-of-slope (Vischkuil-A mudstone, A5-A6 mudstone, and A-B mudstone), lower slope (B-C mudstone) and mid slope (C2-C3 mudstone and C-D mudstone) environments (Figure 1C).

3 | MATERIALS AND METHODS

This study focusses on two continuous cores from research boreholes (BAV 1A and BAV 1B) drilled in the south-west of the Laingsburg depocentre (Baviaans area). The borehole locations are *ca* 475 m apart, but aligned orthogonal to structural dip such that they intersect the Vischkuil, Laingsburg and Fort Brown formations (cumulative thickness of 796 m) (Figure 1). The six regional deep-water mudstone units investigated in this study (Vischkuil-A, A5-A6, A-B, B-C, C2-C3, C-D; Figure 1C) were continuously logged (cumulative thickness of 164 m) graphically through observations of both dry and wet well-polished surfaces of longitudinally split core, using variable lighting, and following the guidelines of Lazar et al. (2015). Logging focussed on the description of macroscopically visible features including: (i) lithology, (ii) colour, (iii) physical sedimentary structures, (iv) bed contacts, (v) bed thicknesses, (vi) deformation, (vii) trace fossils and (viii) bioturbation index. The bioturbation index (BI) was described on a 0–6 scale using the scheme of Taylor and Goldring (1993), where 0 corresponds to non-bioturbated sediment, and 6 corresponds to completely homogenised sediment. The presence of calcium carbonate was assessed by dropping 10% hydrochloric acid (v/v) onto the core surface. The cores were subdivided into different mudstone and sandstone facies based on distinct lithology, primary sedimentary structures, lateral continuity of the beds and
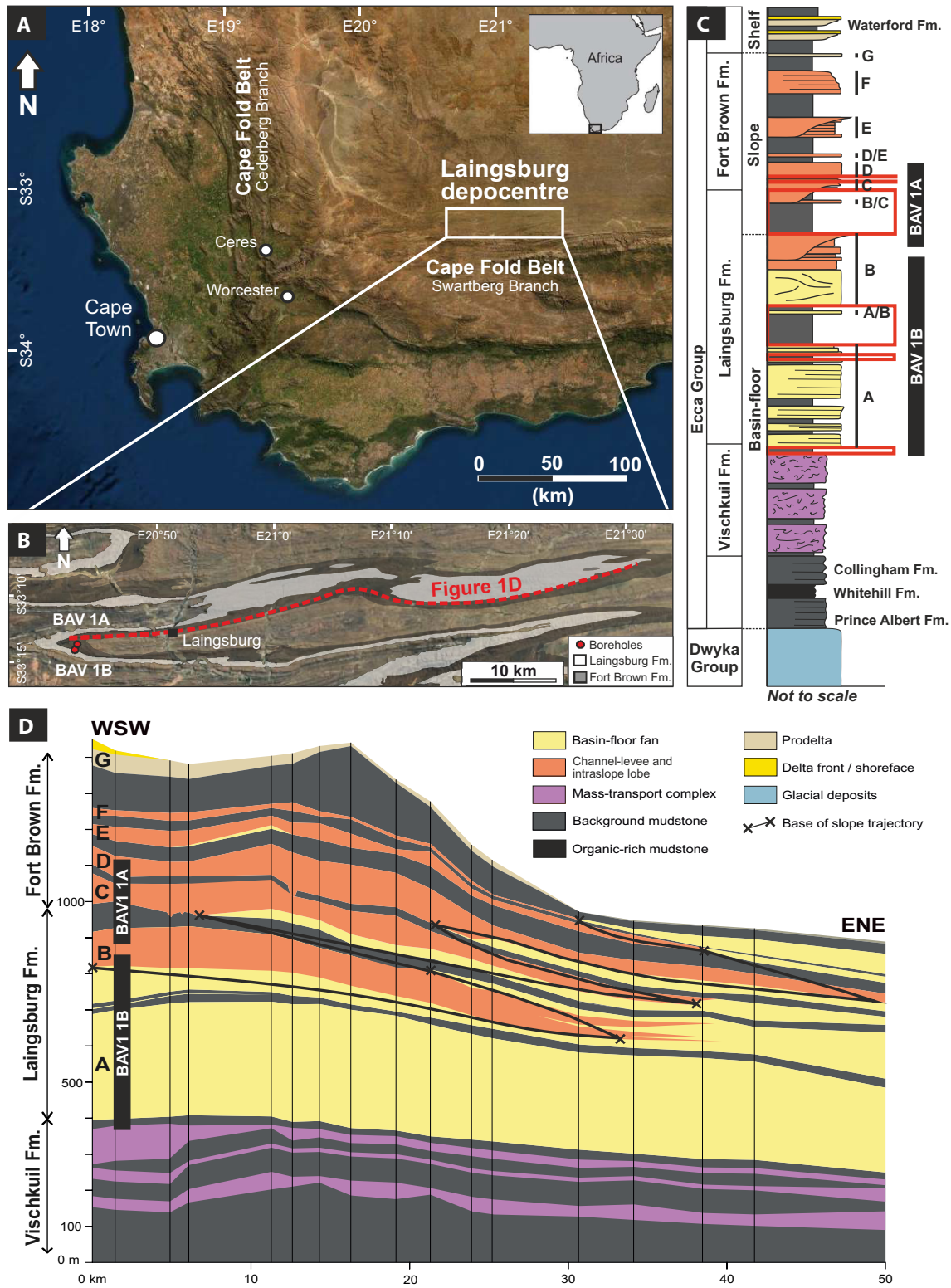
FIGURE 1 (A) Satellite view of south-West South Africa with location of the study area (Laingsburg depocentre, Karoo Basin) indicated by the white square. (B) Satellite view of Laingsburg depocentre showing the outcrop belt of the Permian Laingsburg and Fort Brown formations, and the location of the two cores described in this study (BAV 1A, BAV 1B). (C) Schematic stratigraphic log of the Karoo Supergroup in the Laingsburg depocentre. The six mudstone units presented in this study are indicated by the red rectangles. The stratigraphic package encompassed by the two cores is indicated by the black rectangles. Redrawn after Brooks, Hodgson, Brunt, Peakall, Poyatos-Moré, and Flint (2018a). (D) Stratigraphic correlation of the Upper Ecca Group in the Laingsburg depocentre. The location of the panel is shown in (B). The projected drilling location of the two cores described in this study (BAV 1A, BAV 1B) is indicated. Redrawn after Poyatos-Moré et al. (2019)

bioturbation intensity observed at core scale. Mudstone facies were later refined by observations of microscopic features in thin sections. The sedimentology of the mudstone units was not studied in detail in outcrop because of the poor exposure and a strong pencil-like weathering which prevents the observation of bedding and sedimentary structures.

A total of 56 samples were collected from BAV 1A and BAV 1B using an adjusted uniform sampling spacing method of one sample per 4.5 m, to include every mudstone facies and features of interest (facies contacts, trace fossils, diagenetic features). Thirty samples were selected to represent all mudstone facies described at core scale, and prepared for oriented polished thin sections (24×46 mm) normal to the bedding orientation. Each thin section was scanned using an Epson Perfection V600 flatbed scanner at a resolution of 3200 dpi. Microscopic observations in both plane-polarised light (PPL) and cross-polarised light (XPL) were performed using a Nikon Eclipse LV100NPOL optical microscope fitted with a Nikon DS-Fi2 camera. Microscopic analysis focussed on characterisation of the millimetre-scale variability in sedimentary features (grading, bed contacts, laminae), grain size, composition and bioturbation intensity. Each thin section was logged at sub-millimetre scale, and photomicrographs were taken at different magnifications to record sedimentary structures, bedding and texture. Following the guidelines of Campbell (1967) and Lazar et al. (2015), no thickness cut-off was used to differentiate a bed and a lamination, and individual beds were identified based on the recognition of bedding surfaces, marked by erosion, stratal terminations or changes in bioturbation. Mudstones with more than half the grains <10 µm were classified as fine mudstone, and mudstones with more than half the grains >10 µm as coarse mudstone (McCave et al., 1995). A composition modifier (siliceous, calcareous, argillaceous and carbonaceous) was added depending on the dominant grain type (quartz, carbonate, clay and organic matter respectively). Stratigraphic changes in bioturbation intensity, burrow size and ichnodiversity were used qualitatively to infer palaeo-sea floor physico-chemical conditions (oxygen level, sedimentation rate, frequency of flow events) (Gingras et al., 2011).

Thickness data from the A-B, B-C and C-D mudstone units, obtained by walking out exposures and logging sections across the 2500 km² study area (Figure 1B), were compiled from previous studies (Brunt et al., 2013b; Di Celma et al., 2011; Figueiredo et al., 2010; Van der Merwe et al., 2014). These data were used to produce thickness maps, by plotting the thickness values using the kriging tool within ArcGIS® Geostatistical Wizard. The thicknesses of the A/B and B/C sandstone units (Brooks et al., 2018a) have been subtracted from the A-B and B-C mudstone thickness maps respectively.

4 | FACIES ANALYSIS

Twelve sedimentary facies (F1-F12) were defined based on the BAV 1A and BAV 1B core description. Three mudstone facies (F1-F3) are described in detail and interpreted below (Figures 2 through 8). Nine sandstone-prone facies (F4-F12) are summarised and illustrated in Table 1. These 12 facies stack to form nine facies associations (FA1-FA9), which are summarised in Table 2. The sandstone-prone facies and facies associations are based on previous works (Brooks et al., 2018a; Brunt et al., 2013a, 2013b; Di Celma et al., 2011; Figueiredo et al., 2010; Grecula et al., 2003a, 2003b; Hodgson et al., 2011; Morris et al., 2014a, 2014b; Spychala et al., 2015, 2017; Van der Merwe et al., 2009, 2014), and are used here to contextualise the three-dimensional depositional setting of the regional mudstone units described from the one-dimensional core dataset. Sedimentological logs are presented from the three basin-floor mudstone units (Figure 9), the three slope mudstone units (Figure 10), and representative core sections from basin-floor (Figure 11) and slope mudstones (Figure 12).

4.1 | Facies 1 (F1): Very thin-bedded mudstone

Facies 1 (F1) consists of light-grey to mid-grey, siliceous–argillaceous, fine to coarse mudstone with well-developed bedding (Figure 2A–C). Beds are laterally continuous at core scale, and range in thickness from 0.04 to 1 cm (very thin bedded sensu Campbell, 1967) (Figures 2A, 11E and 12E). Bioturbation in F1 is sparse to moderate (BI: 1–3), and usually increases upward at bed scale. Individual trace fossils are readily recognised due to lithological contrasts between burrow fill and surrounding sediment (Figures 11E and 12E). Ichnotaxa consist mainly of *Helminthopsis* and *Phycosiphon*, with rare *Planolites*, which are generally <0.5 cm in diameter (Figures 11D,E and 12E,F).

To capture the variability of grading patterns and physical sedimentary structures recognised at thin-section scale, beds within the thin sections of F1 have been subdivided into six different bed types (Bed types A–F; Figures 3 and 4), which are described and interpreted below.

4.1.1 | Bed type A

Description—Bed type A exhibits sharp to erosional bed bases, with rare flame and load structures, and a bipartite microstratigraphy (Figures 3A and 4). The lower microstratigraphic subdivision is normally graded, with rare laterally continuous to discontinuous planar-parallel laminae (Figures 3A and 4). The upper subdivision is mottled
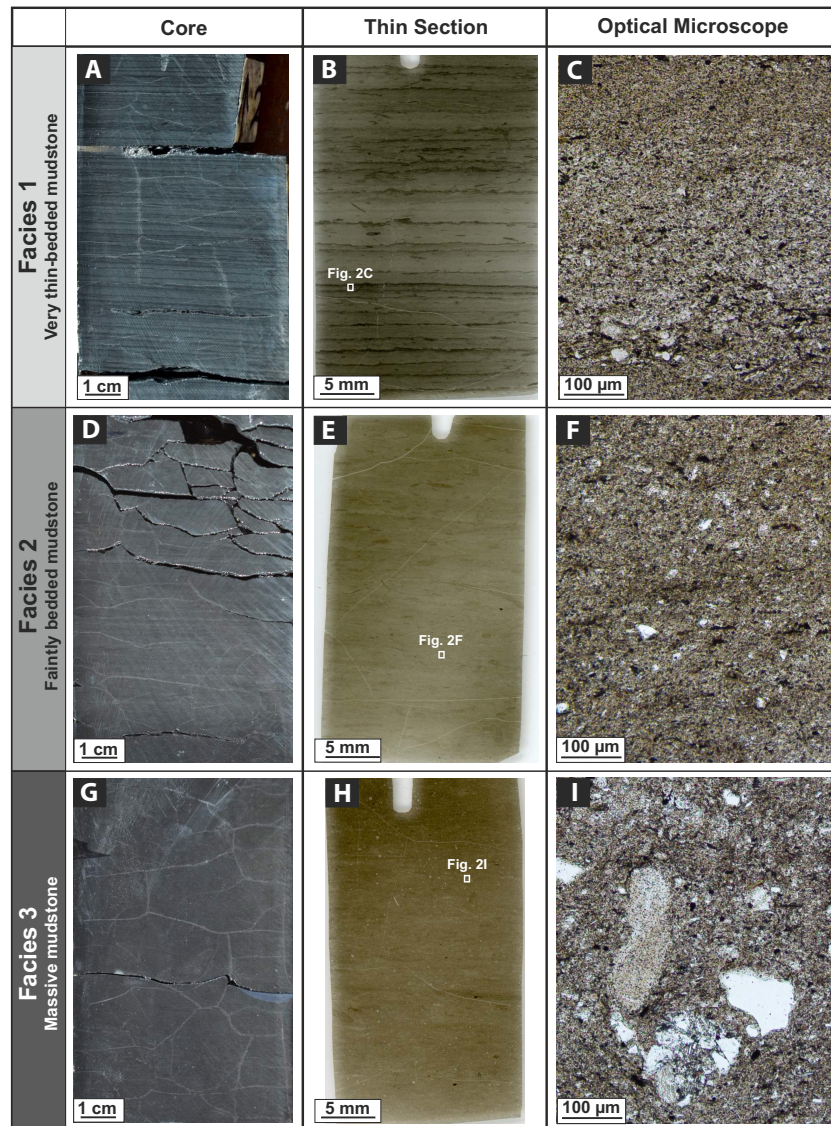
FIGURE 2 Illustrations of the three mudstone facies identified in BAV 1A and BAV 1B cores. (A) Wet core photograph of Facies 1 (very thin-bedded mudstone) characterised by stacked millimetre-thick beds laterally continuous at core scale (BAV 1B; 211.63 m). (B) Thin section scan showing variably graded stacked very thin beds of Facies 1. (C) Photomicrograph (PPL) of the texture of Facies 1 with a normally graded bed. (D) Wet core photograph of Facies 2 (faintly bedded mudstone) characterised by stacked millimetre-thick bioturbated beds laterally discontinuous at core scale (BAV 1B; 198.46 m). (E) Thin section scan showing stacked bioturbated beds. Note the gradational bed boundaries due to bioturbation. (F) Photomicrograph (PPL) of the texture of Facies 2. Texture is poorly sorted because of bioturbation. (G) Wet core photograph of Facies 3 (massive mudstone) characterised by a massive texture at core scale (BAV 1B; 172.80 m). (H) Thin section scan showing a 'starry-night' texture. (I) Photomicrograph (PPL) of the texture of Facies 3. Texture consists of floating outsized very fine to medium sand size particles (mudstone clasts, quartz, volcanic rock fragments) in a matrix of poorly-sorted mud. White squares in thin-section scans indicate locations of photomicrographs

(Figure 3A). Rare normally graded beds are characterised by a more complex microstratigraphy, with a basal lenticular laminated subdivision, overlain by convolute and planar-parallel laminae, and capped by a mottled subdivision (Figure 4B).

Interpretation—Based on the presence of normal grading and planar parallel to lenticular laminae, Bed type A is interpreted to represent deposition from waning, low-density turbidity currents (sensu Lowe, 1982). The sharp to erosional bases suggest incision and/or by-pass of the frontal part of the forming or preceding flow (Stevenson et al., 2015). The lower normally graded bed subdivision with occasional planar-parallel and lenticular laminae suggests deposition under tractional currents (Piper, 1978; Stow & Shanmugam, 1980). The upper mottled subdivision is indicative of suspension fallout.

FIGURE 3 Representative photomicrographs (PPL), descriptions, and process interpretations of the six bed types identified in Facies 1 (very thin-bedded mudstone). (A) Bed type a is normally graded, and interpreted as deposited by waning, low-density turbidity current (BAV 1B; 505.25 m). (B) Bed type B is inversely graded, and interpreted as deposited by waxing, low-density turbidity current. (C) Bed type C is inversely to normally graded, and interpreted as deposited by waxing-to-waning, low-density turbidity currents (BAV 1B; 505.25 m). (D) Bed type D is characterised by stacked normally graded laminae, and interpreted as deposited by multi-pulsed, low-density turbidity currents (BAV 1B; 198.79 m). (E) Bed type E exhibits an internal bipartite microstratigraphy, and is interpreted as deposited by transitional flows or co-genetic turbidity currents and cohesive debris flows (BAV 1B; 167.57 m). (F) Bed type F grading and sedimentary structures are not preserved due to strong bioturbation. This type of bed may have been primarily deposited by any of the processes responsible for the accumulation of bed types A–D before intense reworking by bioturbation (BAV 1A; 240.91 m)

The occurrence of convolute laminae suggests loading into unconsolidated mud (Stow & Shanmugam, 1980).

4.1.2 | Bed type B

Description—Bed type B exhibits inverse grading and is characterised by a gradational base, and a sharp upper contact (Figure 3B). Sedimentary structures consist of laterally continuous to discontinuous planar-parallel laminae located in the upper part of the bed (Figure 3B).

Interpretation—The inversely graded characteristic of Bed type B suggests deposition to have occurred as a result of waxing, low-density turbidity currents, with evidence for traction transport (Kneller & McCaffrey, 2003; Mulder & Alexander, 2001). The occurrence of a sharp upper bed contact, in addition to the absence of overlying normally

FIGURE 4 Thin-section scans illustrating the bed stacking pattern of Facies 1 (very thin-bedded mudstone). (A) Basin floor, Vischkuil-A mudstone (BAV 1B; 505.25 m). Note the dominance of graded laminated beds (bed type D), and the inversely to normally graded beds (bed type C) near the top. (B) Base-of-slope, A-B mudstone (BAV 1B; 167.57 m). Note the dominance of normally graded beds (bed type A). (C) Lower slope, B-C mudstone (BAV 1B; 198.79 m). Note the dominance of graded laminated beds (Bed type D). (D) Mid slope, C–D mudstone (BAV 1A; 72.50 m). Note the dominance of bioturbated beds (bed type F), with rare intercalated normally graded (bed type A) and graded laminated (bed type D) beds
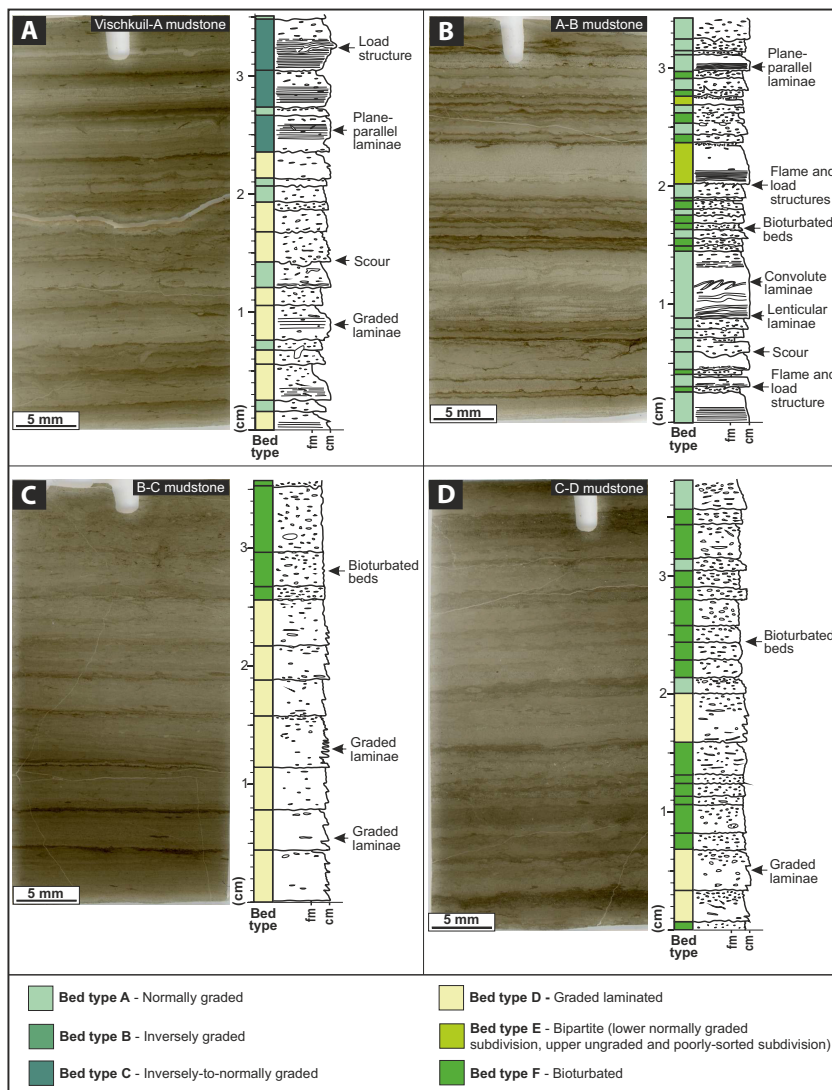
graded deposits, suggest sediment bypass (Poyatos-Moré et al., 2016; Stevenson et al., 2015), similar to the incomplete hyperpycnites of Mulder et al. (2003).

4.1.3 | Bed type C

Description—Bed type C shows a sharp to erosional base, with rare flame and load structures (Figure 3C). This type of bed is inversely to normally graded, and sedimentary structures include laterally continuous to discontinuous planar-parallel laminae (Figure 3C). The upper part of the bed is generally mottled.

Interpretation—The sharp to erosional base suggests incision and/or bypass of the frontal part of the forming or preceding flow (Stevenson et al., 2015). The flame and load structures and inverse-to-normal grading motif of Bed type C suggests relatively rapid deposition from sustained, waxing-to-waning, low-density turbidity currents (i.e. hyperpycnal flows) (Mulder et al., 2003; Mulder & Alexander, 2001).

4.1.4 | Bed type D

Description—Bed type D is characterised by a sharp to erosional base, with rare flame and load structures (Figure 3D). Internal bed structure consists of stacked normally graded laminae (<1 mm thick), with gradational or sharp contacts (Figures 3D and 4C). Laminae are either thinning and fining upward or thickening and coarsening upward within individual beds (Figure 4C).

Interpretation—The stacking of normally graded laminae and the several types of grading observed within Bed type D suggests deposition from pulsating, low-density turbidity currents, with internal flow fluctuations (Ho et al., 2018).

4.1.5 | Bed type E

Description—Bed type E is characterised by a sharp to erosional base, with rare flame and load structures
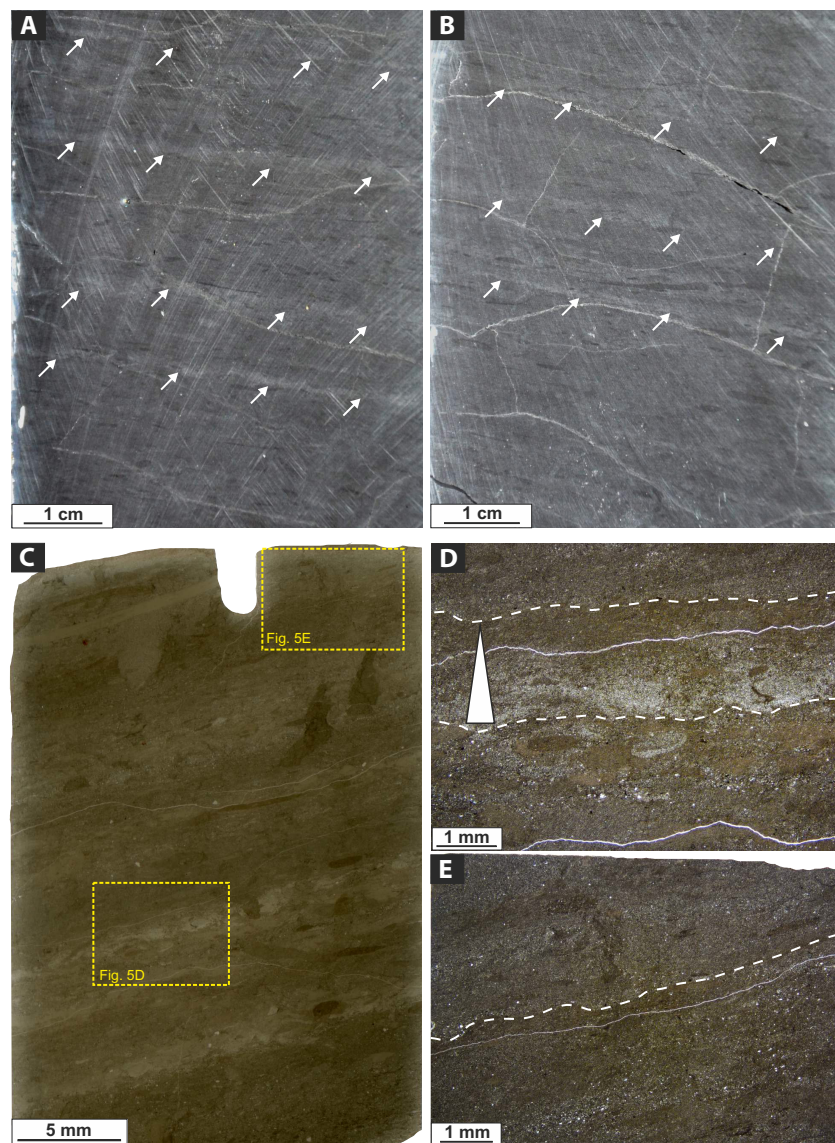
FIGURE 5 Examples of the key features of Facies 2 (faintly bedded mudstone). (A) Wet core photograph of laterally discontinuous very thin beds. White arrows indicate the base of mudstone beds (BAV 1A; 231.10 m). (B) Wet core photograph of laterally discontinuous very thin beds. White arrows indicate the base of mudstone beds (BAV 1A; 217.35 m). (C) Thin section of stacked laterally discontinuous very thin beds (BAV 1A; 79.10 m). (D) Photomicrograph (PPL) of preserved normally graded bed. (E) Photomicrograph (PPL) of a bioturbated mudstone bed. Location of part D and E are shown in part C

(Figure 3E). This type of bed displays a bipartite microstratigraphy (Figure 3E). The lower subdivision is normally graded with laterally continuous to discontinuous planar-parallel laminae (Figure 3E). The upper subdivision is ungraded and characterised by a poorly sorted muddy matrix that supports outsized very fine to fine sand size grains (quartz, altered feldspars, volcanic and metamorphic rock fragments, mudstone clasts) (Figure 3E).

Interpretation—The sharp to erosional base suggests incision and/or bypass of the frontal part of the forming or preceding flow (Stevenson et al., 2015). The bipartite organisation of Bed type E with a lower normally graded subdivision, overlain by an ungraded and poorly sorted subdivision suggests deposition from strongly stratified transitional flows (Baas et al., 2011; Kane & Pontén, 2012), or from co-genetic turbidity currents (lower subdivision)

and cohesive debris flows (upper subdivision) (Haughton et al., 2003).

4.1.6 | Bed type F

When a bed type within F1 could not be determined confidently due to the presence of moderate bioturbation, but the bed is laterally continuous at core scale and stratification is preserved, the bed was assigned to Bed type F (Figures 3F and 4). The absence of preserved grading and sedimentary structures in Bed type F, and its stratigraphic association with the other bed types of F1, suggest primarily deposition by any processes responsible for the accumulation of Bed types A–D (waning, waxing-to-waning, waxing, or pulsating low-density turbidity currents), prior to biogenic reworking, overprinting pre-existing grading and sedimentary structures.
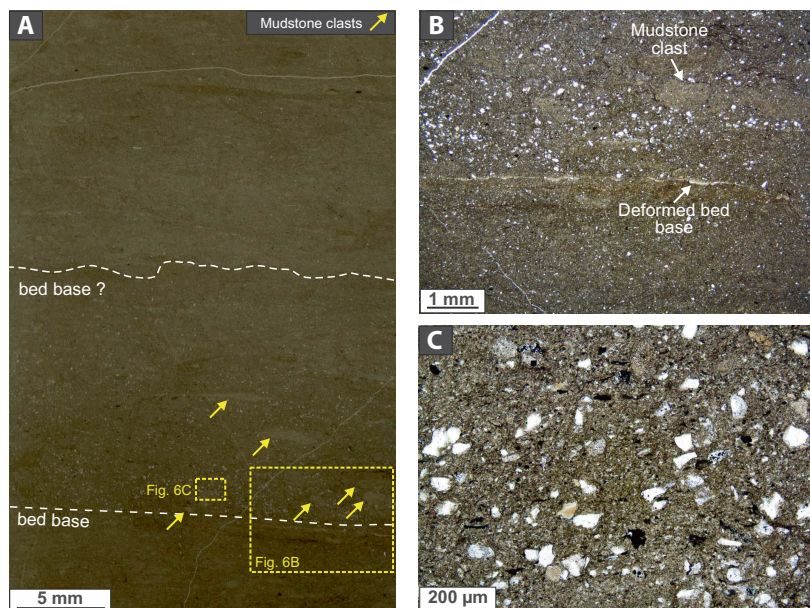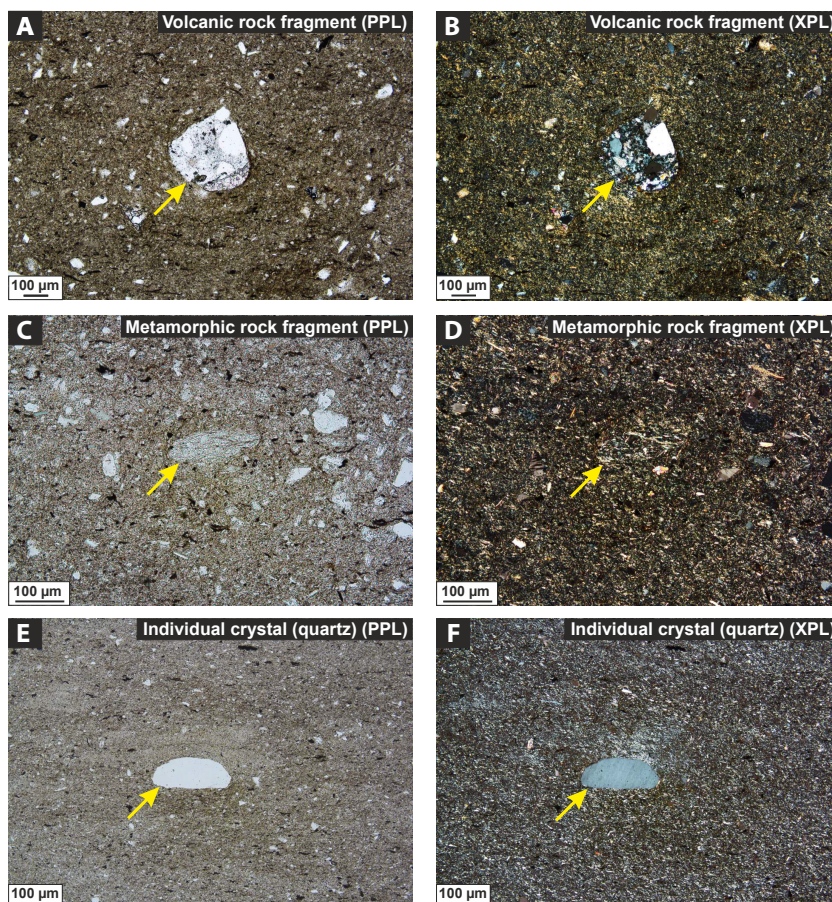
FIGURE 6 Example of Facies 3 (massive mudstone) with a 'starry-night' texture (BAV 1A; 219.25 m). (A) Thin-section scan. Note the 'starry-night' texture in the bed interpreted as deposited from low-strength, cohesive debris flow, prior to intense post-depositional bioturbation. (B) Photomicrograph (PPL) showing a zoomed in view of the dashed square in part A. Note the example of a deformed bed base, and the poorly sorted texture. (C) Photomicrograph (PPL) showing a zoomed in view of the dashed square in part A, and illustrating the poorly sorted texture within the bed. Mineralogy consists of quartz and feldspar crystals, volcanic and metamorphic rock fragments, and mudstone clasts

FIGURE 7 Photomicrographs showing examples of different types of outsized particles (yellow arrows) identified in thin sections of Facies 3 (massive mudstone). (A, B) Volcanic rock fragment of medium sand size in a matrix of mud (PPL and XPL) (BAV 1B; 172.80 m). Note the differential compaction around the outsized particle. (C, D) Metamorphic rock fragment of fine sand size in a matrix of mud (PPL and XPL) (BAV 1B; 172.80 m). Note the foliations within the fragment. (E, F) Crystal of quartz of fine sand size in a matrix of mud (PPL and XPL) (BAV 1B; 203.10 m)
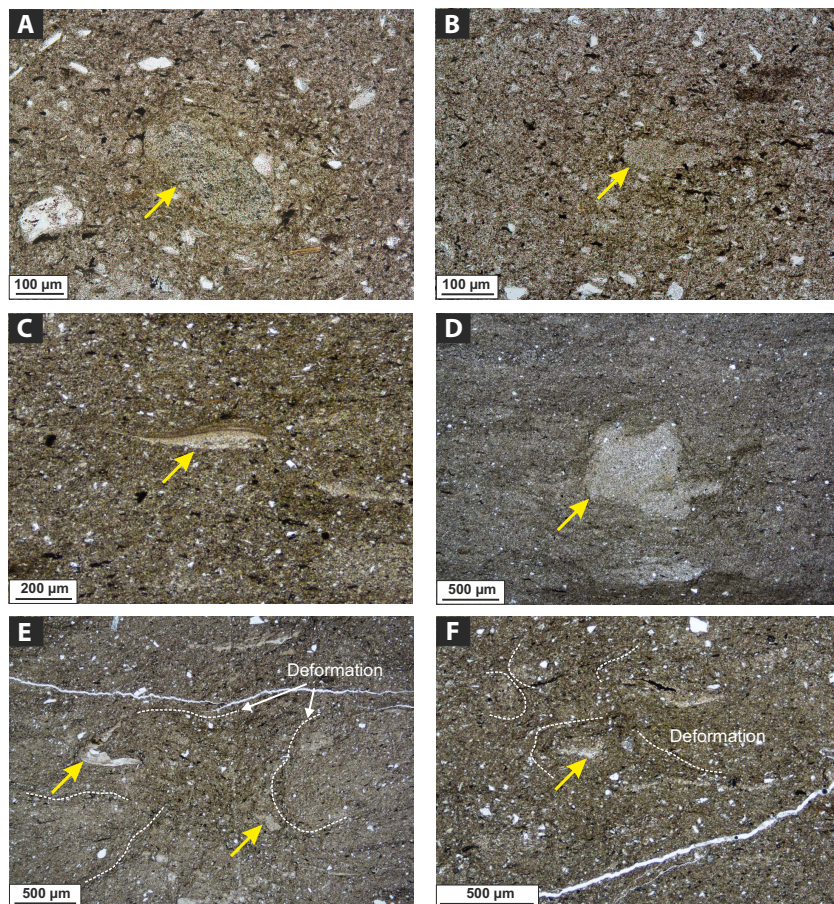
FIGURE 8 Photomicrographs (PPL) showing examples of mudstone clasts (yellow arrows) and deformations (white dotted lines) identified in thin sections of Facies 3 (massive mudstone). (A) Rounded mudstone clast in a matrix of mud (BAV 1B; 172.80 m). (B) Sub-rounded mudstone clast in a matrix of mud (BAV 1B; 172.80 m). (C) Sub-angular mudstone clast in a matrix of mud (BAV 1B; 203.10 m). (D) Mudstone clast characterised by plastic deformations in a matrix of mud (BAV 1B; 181.85 m). (E) Deformation within F3 (BAV 1B; 177.81 m). Note the highly deformed mudstone clast to the left. (F) Deformation in F3 (BAV 1A; 224.15 m)

4.2 | Facies 2 (F2): Faintly bedded mudstone

4.2.1 | Description

Facies 2 (F2) consists of light-grey to mid-grey, siliceous–argillaceous, fine to coarse grained mudstone with poorly developed bedding (Figures 2D,E,F and 5). Beds in F2 range in thickness from 0.03 to 1 cm (very thin bedded sensu Campbell, 1967), but are typically <0.5 cm thick (Figure 5). Bioturbation in F2 is moderate to high (BI: 3–4), and beds are distinctively laterally discontinuous at core scale, with poorly defined bed boundaries (Figures 2D, 5A,B, 11D and 12B). At microscopic scale, no sedimentary structures are identified (Figures 2E and 5C,D,E). Grading is usually obscured by moderate to high bioturbation, but rare normally graded beds are preserved (Figure 5D). Individual trace fossils are readily recognised due to grain-size contrasts between burrow-fill and host bed, and burrows are usually larger than in F1 (<1 cm in diameter in F2 versus <0.5 cm in F1) (Figures 11B,D and 12B). Ichnotaxa consist mainly of *Helminthopsis* and *Phycosiphon*, with rare *Chondrites*, *Nereites* and *Planolites* (Figures 11B,D and 12B).

4.2.2 | Interpretation

Remnant bedding suggests F2 was deposited by sediment gravity flows. Rare preserved normally graded beds suggest deposition from dominantly waning, low-density turbidity currents (sensu Lowe, 1982). The higher bioturbation intensity, higher ichnodiversity and larger burrows in F2 compared to F1 suggest less physico-chemically stressed conditions for organisms, potentially linked to lower sedimentation rates, longer depositional breaks and/or variation in the geochemistry of bottom waters and porewaters (Gingras et al., 2011; Heard & Pickering, 2008; Wetzel, 1984).

4.3 | Facies 3 (F3): Massive mudstone

4.3.1 | Description

Facies 3 (F3) consists of mid-grey to dark-grey, argillaceous–siliceous, fine to coarse grained mudstone (Figure 2G,H,I). In comparison to F1 and F2, F3 is characterised by a massive texture at core scale (Figures 2G, 11B,C,D and 12C). At microscopic scale, F3 exhibits a 'starry-night' texture (Haughton et al., 2003), which

TABLE 1 Sandstone-prone facies description (F4–F12), process interpretation, and representative core photographs
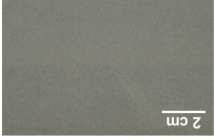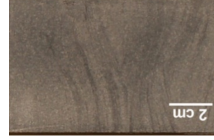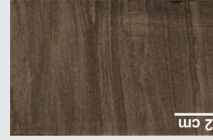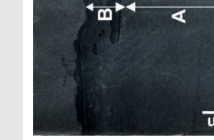
Facies name	Grain size	Bed thickness range	Description	BI	Depositional processes	Core photograph
Structureless sandstone (F4)	Very fine to fine sand	10–200 cm	Structureless. Occasional dewatering pipes and dishes. Sharp, erosional or loaded bases. Common flute and tool marks. Sharp tops	0	High-density turbidites: Massive structuration suggests deposition from highly concentrated flow (Kneller & Branney, 1995; Lowe, 1982) with high sediment load fallout (Arnott & Hand, 1989)	
Structured sandstone (F5)	Very fine to fine sand	5–70 cm	Planar, current-ripple or low-angle climbing-ripple lamination. Sharp or loaded bases. Sharp or gradational tops, commonly undulating. Mudstone drapes	0–2	Low-density turbidites: Planar and current-ripple lamination produced by tractional reworking of bed tops by dilute flows (Allen, 1982; Best & Bridge, 1992). Climbing-ripple lamination forms under bedload transport associated with high aggradation rates (Hunter, 1977; Jobe et al., 2012)	
Sigmoidal sandstone (F6)	Very fine sand	2–30 cm	Sigmoidal shaped bedform with sinusoidal lamination. Stoss-side preserved climbing ripple lamination. Current-ripple, planar or low-angle ripple lamination. Sharp bases. Gradational tops	0–2	Low-density turbidites: Sinusoidal and climbing-ripple lamination associated with high rates of deposition (Hunter, 1977; Jobe et al., 2012). Deposited from flows escaping confinement and depositing rapidly (Morris et al., 2014b)	
Interbedded sandstone and mudstone (F7)	Coarse mud to very fine sand	1–15 cm	Very fine sandstones include wavy, aggradational, planar, current-ripple, climbing and stoss-side preserved climbing ripple lamination. Mudstone drapes with planar laminae. Gradational or sharp bases. Often gradational tops	0–3	Low-density turbidites: Planar and current-ripple lamination produced by tractional reworking of bed tops by dilute flows (Allen, 1982; Best & Bridge, 1992). Climbing-ripple lamination forms under bedload transport associated with high aggradation rates (Hunter, 1977; Jobe et al., 2012). Wavy lamination associated with waning flows and high rates of suspension fallout (Hunter, 1977; Jopling & Walker, 1968). Mud deposited by the dilute tail of the flow	
Hybrid event bed (F8)	Fine mud to very fine sand	20–150 cm	Two subdivisions. Lower subdivision (A) well sorted and 'clean' sandstone. Upper subdivision (B) can be: (1) mudstone-clast rich with 'clean' matrix; (2) argillaceous, poorly sorted sandstone with swirly and patchy fabric comprising mudstone chips and wood fragments. Sharp or erosional bases. Sharp tops	0–3	Hybrid event beds: Strongly stratified transitional flows (Baas et al., 2011; Kane & Pontén, 2012) or co-genetic turbidity currents (lower subdivision) and cohesive debris flows (upper subdivision) (Haughton et al., 2003)	

TABLE 1 (Continued)
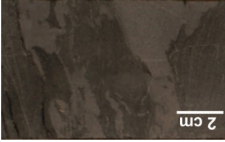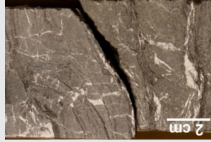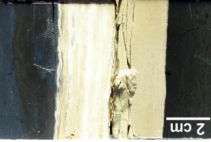
Facies name	Grain size	Bed thickness range	Description	BI	Depositional processes	Core photograph
Mudstone clast conglomerate (F9)	Fine sand	1–10 cm	Tightly packed mudstone clasts draping erosive surfaces. From high concentration clast supported to matrix supported conglomerate. Sharp and erosional bases, normally planar with local topography related to the substrate erodibility	0	Channel lags/drapes: Mudclasts transported in traction beneath confined flows and deposited as channel lag/drape	2 cm
Chaotic deposits (F10)	Fine mud to fine sand	0.5 cm to several m	Contorted sandstone clasts supported by a poorly sorted mudstone-prone matrix. Other packages are poorly sorted and contain dispersed sub-angular, elongate, mm-cm scale mudstone clasts and plant fragments. Occasional dewatering structures. Sharp bases and tops	0–3	Debrites: *En masse* freezing of cohesive debris flows (Iverson, 1997; Nardin et al., 1979)	2 cm
Folded deposits (F11)	Fine mud to fine sand	10 cm-10s of m	Contorted and folded clasts (cm to 10's cm scale) with syn-sedimentary faults. Internal bedding well preserved within clasts. Dewatering structures. Gradational to sharp bases and tops	0	Slumps/slides: Folded strata formed as slumps and slides remobilise primary bedding, undergoing ductile deformation. Clast formed as cohesive material is remobilised as slides and undergoing only brittle deformation	2 cm
Ash-rich sandstone (F12)	Very fine to fine sand	2–30 cm	Planar and current-ripple lamination. Normally graded or ungraded. Sharp or erosional bases. Brownish to greenish colour	BI: 1–3	Low-density turbidites/tuffs: Normally graded bed deposited by low-density turbidity currents. Ungraded beds deposited by vertical suspension fallout	2 cm

TABLE 2 Facies associations (FA1–FA9) descriptions

FA code	Facies association name	Common facies	Main characteristics
Sandstone-prone FA			
FA1	Proximal lobe (axis to fringe)	Structureless sandstone (F4), structured sandstone (F5), sigmoidal sandstone (F6), interbedded sandstone and mudstone (F7), bipartite bed (F8), mudstone clast conglomerate (F9), chaotic deposits (F10)	10's of cm to a few m thick. Tabular-shape deposits. Decrease of sand content from axis to fringe. *Axis*: directly downdip of the feeder channel, common erosion, bypass and bed amalgamation. *Off-axis*: Alternation of bedded sandstones and mudstones. *Fringe*: Lower sand content; alternation of bedded sandstones and mudstones with common hybrid event beds (F8) in frontal position
FA2	Distal lobe (distal fringe)	Very thin-bedded mudstone (F1), faintly bedded mudstone (F2), interbedded sandstone and mudstone (F7), ash-rich sandstone (F12)	Few cm to a few m thick. Tabular-shape deposits that correlate laterally to proximal lobe deposits. Very thin-bedded mudstone (F1) deposited in more proximal environment compared to faintly bedded mudstone (F2)
FA3	Channel fill	Structureless sandstone (F4), structured sandstone (F5), interbedded sandstone and mudstone (F7), mudstone clast conglomerate (F9), folded deposits (F11)	Few m thick. Lens shape deposits filling concave-up surfaces. Axial zones with repeated phases of erosion/deposition and common amalgamation and bypass surfaces. Gradual thinning and fining away from axial zone, with low angle erosional surfaces identified through bed truncation
FA4	Levee	Sigmoidal sandstone (F6), interbedded sandstone and mudstone (F7)	Few m to 10's of m thick. Wedge-shape geometry away from channel over 100's of m. Fining and thinning-upward rhythmic alternations. Deposits closer to coeval channel exhibit highly tractional and rapidly deposited structures, often recording multi-directional current ripple and climbing ripple lamination. Sandstone content decreases non-linearly away from the channel
FA5	Intraslope frontal lobe	Structured sandstone (F5), sigmoidal sandstone (F6), interbedded sandstone and mudstone (F7), bipartite bed (F8)	Few m thick. Mounded geometry. High rates of suspension fallout linked to rapid flow expansion and deposition directly downdip of slope channels
FA6	Remobilised	Chaotic deposits (F10), folded deposits (F11)	Few m thick. Chaotic and remobilised deposits filling slide scars and topography created by mass-transport deposits
Mudstone-prone FA			
FA7	Basin-floor mudstone bedset	Very thin-bedded mudstone (F1), faintly bedded mudstone (F2), interbedded sandstone and mudstone (F7), ash-rich sandstone (F12)	Few cm to a few m thick (up to 1.7 m thick). Do not correlate laterally to any sandstones on the basin-floor. Most dominant bed type of F1 is graded laminated (*Bed type D*), followed by normally graded (*Bed type A*), bioturbated (*Bed type F*), inversely to normally graded (*Bed type C*), bipartite (*Bed type E*) and inversely graded (*Bed type B*). Rare ash-rich sandstones (F12) and carbonate-rich concretions

TABLE 2   (Continued)

FA code	Facies association name	Common facies	Main characteristics
FA8	Slope mudstone bedset	Very thin-bedded mudstone (F1), faintly bedded mudstone (F2), ash-rich sandstone (F12)	Few cm to few m thick (up to 8 m thick). Do not correlate laterally to any sandstones on the slope. Most dominated bed type of F1 is bioturbated (*Bed type F*), followed by normally graded (*Bed type A*), graded laminated (*Bed type D*), inversely to normally graded (*Bed type C*) and inversely graded (*Bed type B*). Common ash-rich sandstones (F12) and carbonate-rich concretions. Higher bioturbation intensity and larger burrows compared to FA7
FA9	Massive mudstone package	Massive mudstone (F3), ash-rich sandstone (F12)	Few cm to few m thick. Packages of massive mudstones are thicker in the basin-floor compared to the slope

consists of outsized very fine to medium sand sized particles supported by a poorly sorted matrix of fine to coarse grained mudstone (Figures 2H,I, 6, 7 and 8). Outsized particles consist of sub-rounded to sub-angular individual crystals (quartz, feldspars) and composite particles (volcanic and metamorphic rock fragments, mudstone clasts) (Figures 7 and 8). Mudstone clasts are recognised based on sharp edges, differential compaction around them, and/or different internal grain orientation, and are characterised by the same composition as the surrounding matrix (Figure 8). Rarely, F3 exhibits microdeformations, marked by circular and arcuate grain alignment (Figure 8E,F). Some mudstone clasts also exhibit plastic deformations (Figure 8D,E). Rare bedding contacts are identified in thin sections, and beds are less than 2 cm thick and ungraded (Figure 6A). Bioturbation is intense to complete (BI: 5–6), and individual trace fossils are usually hard to identify due to the lack of lithological contrasts (Figure 2G). However, observations of wet core surfaces allowed identification of a similar trace fossil assemblage as F2, which consists of *Chondrites*, *Helminthopsis*, *Nereites*, *Phycosiphon* and *Planolites*, which are generally <2 cm in diameter (Figures 11B,C and 12C).

4.3.2 | Interpretation

The outsized very fine to medium sand-sized particles supported by a poorly sorted mud matrix suggests F3 was deposited from either: (1) suspension fallout through the water column as dropstones of glacial (ice-rafted debris) or non-glacial origins (e.g. gastroliths, vegetation rafting, aeolian transport) (Bennett et al., 1996); or (2) low-strength, cohesive debris flows, in which sand-sized particles were not vertically segregated from mud particles during deposition (Talling et al., 2012). The rare preserved bed contacts, the poorly sorted mud matrix, and the microdeformations support the interpretation of F3 as low-strength, cohesive debris flow deposits (i.e. debrites), which were subsequently biogenically reworked. The similar composition of the mudstone clasts and the mud matrix suggests clasts are derived from up-dip erosion of partially consolidated sea floor mud (Boulesteix et al., 2019; Fonnesu et al., 2016; Haughton et al., 2003; Patacci et al., 2014; Schieber et al., 2010; Talling et al., 2004). Some of the mudstone clasts are relatively well-rounded (Figure 8A,B), which suggest progressive disintegration and abrasion in sediment gravity flows with a component of turbulence (Boulesteix et al., 2019; Fonnesu et al., 2015; Haughton et al., 2003). Therefore, it is proposed that some of the massive mudstones (F3) may represent the distal expression of flows that underwent transformation from turbulent to laminar along their flow path (Baas et al., 2011; Baker & Baas, 2020; Kane et al., 2017). The intense to complete bioturbation of F3 suggests deposition under a lower sedimentation rate when compared to F1 and F2, associated with a relatively low frequency of flow events (Gingras et al., 2011; Heard & Pickering, 2008; Wetzel, 1984).

5 | STACKING PATTERNS AND DEPOSITIONAL ARCHITECTURE

The description of the facies and facies associations (Tables 1 and 2) provides the sedimentological building blocks to describe the stacking patterns of the six mudstone units analysed (Figures 9 and 10). The stratigraphic
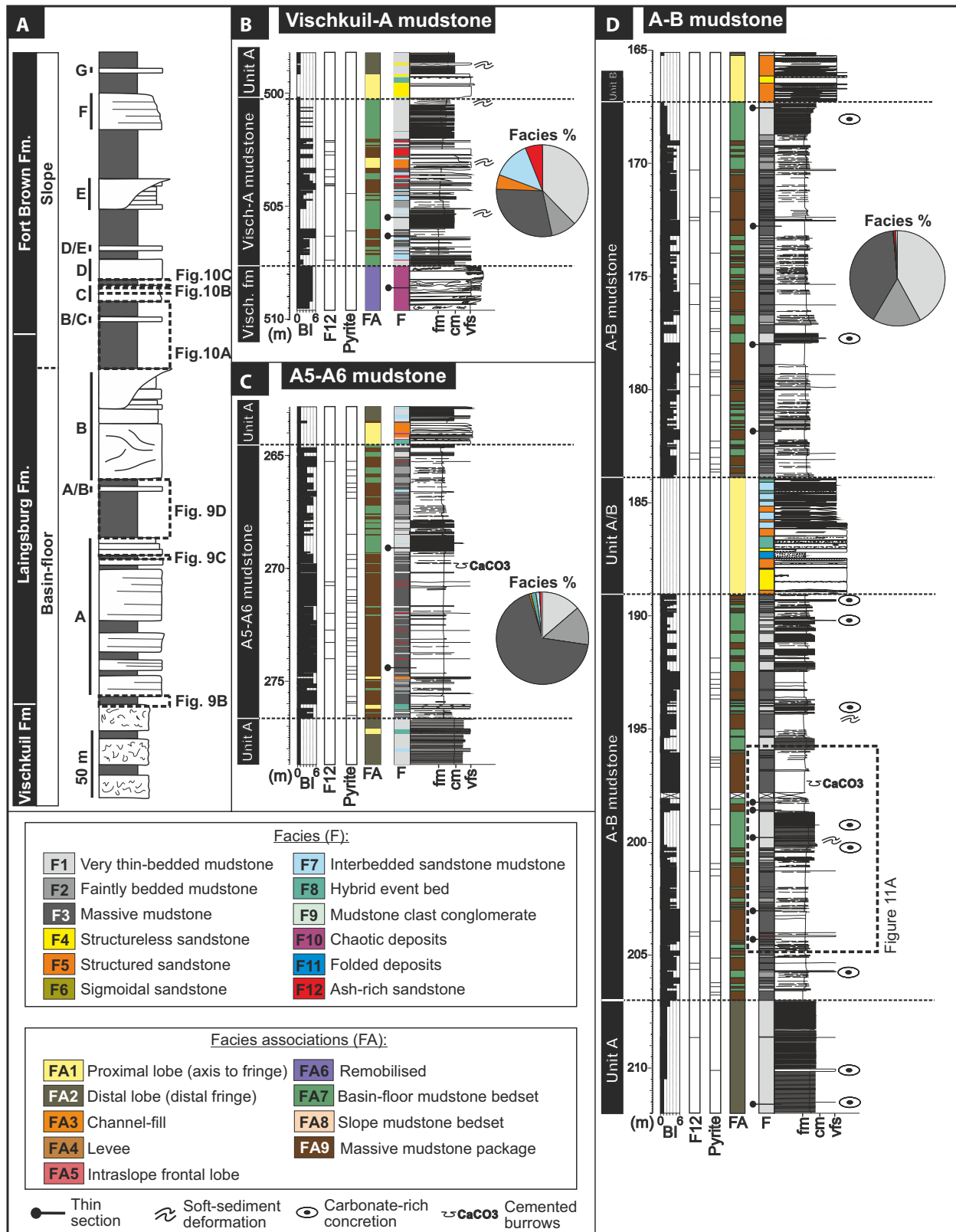
FIGURE 9 Sedimentological logs and facies abundance of the three basin-floor to base-of-slope mudstone units (from BAV 1B). (A) Schematic stratigraphic log of the Upper Ecca Group from the Laingsburg depocentre, with locations of the studied regional mudstone units. (B) Basin floor, Vischkuil-A mudstone unit. (C) Basin floor, A5-A6 mudstone unit. (D) Basin-floor to base-of-slope, A–B mudstone unit. The pie chart represents facies percentage for the entire A-B mudstone unit. Logs include facies (F), facies associations (FA), bioturbation index (BI), presence of pyrite nodules, presence of ash-rich sandstones (F12), and locations of thin sections. Fm = fine mudstone, cm = coarse mudstone, vfs = very fine sandstone
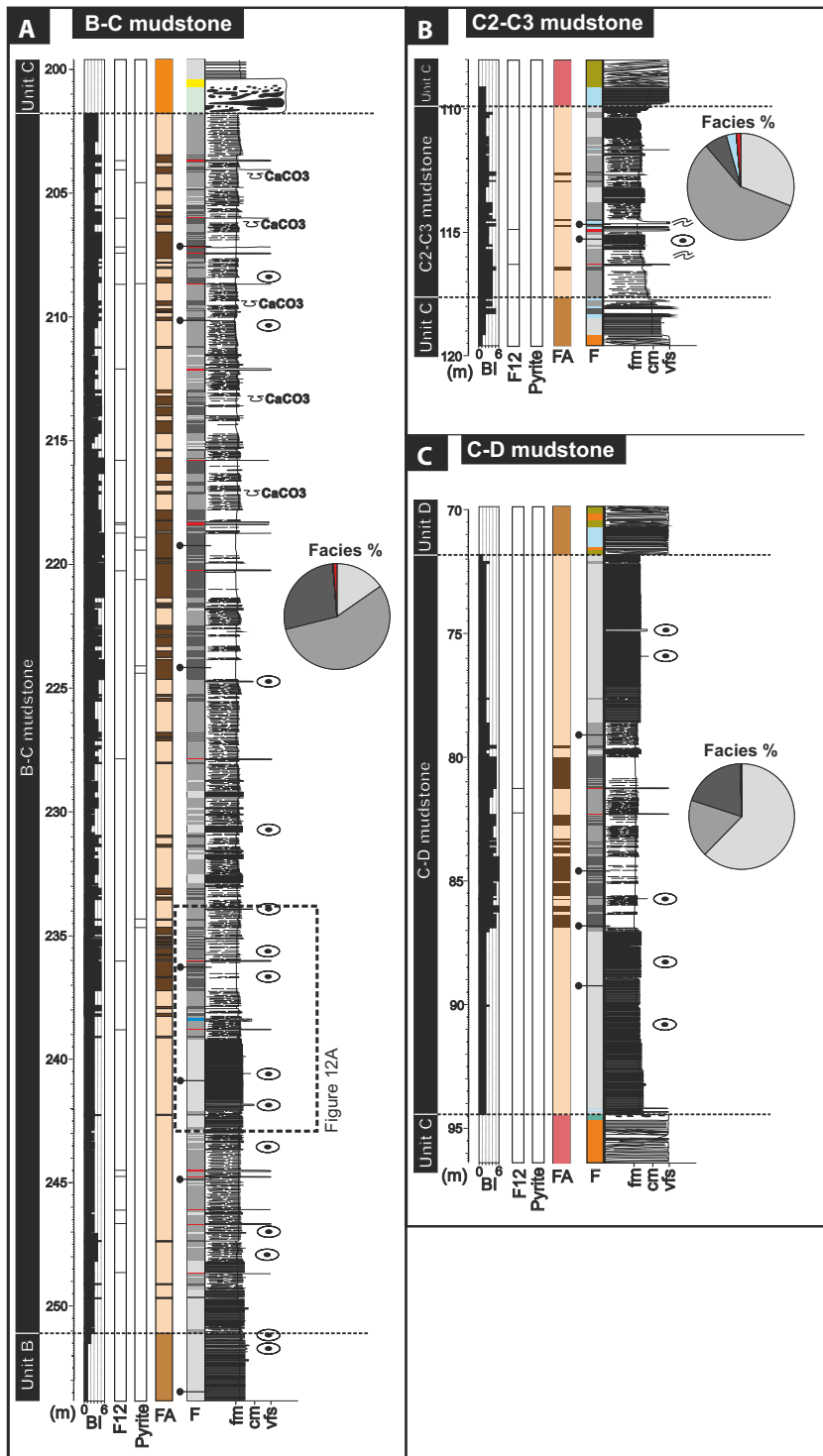
FIGURE 10 Sedimentological logs of the three slope mudstone units (from BAV 1A). See stratigraphic locations in Figure 9A. See legend in Figure 9. (A) Lower slope, B-C mudstone unit. (B) Mid slope, C2-C3 mudstone unit. (C) Mid slope, C-D mudstone unit. Logs include facies (F), facies associations (FA), bioturbation index (BI), presence of pyrite nodules, presence of ash-rich sandstones (F12), and locations of thin sections. Fm = fine mudstone, cm = coarse mudstone, vfs = very fine sandstone

distribution of the facies and the bed types of F1 are summarised in Figure 13. The thickness maps of the A-B, B-C and C-D mudstone units are presented in Figure 14.

5.1 | Basin-floor mudstones

The Vischkuil Formation is dominated by debrites and turbidites accumulated in a distal basin-floor environment (Van der Merwe et al., 2009, 2010), and the overlying Unit A and Unit A/B of the Laingsburg Formation are dominated by basin-floor fan to base-of-slope deposits (Brooks et al., 2018a; Grecula et al., 2003a; Prélat & Hodgson, 2013; Sixsmith et al., 2004). This suggests that the intercalated Vischkuil-A (Figure 9B), A5-A6 (Figure 9C) and A-B (Figure 9D) mudstone units were probably deposited in a similar basin-floor to base-of-slope environment.

FIGURE 11 (A) Representative 9.26 m thick core section and sedimentological log of the basin-floor to base-of-slope A-B mudstone unit (BAV 1B; see Figure 9 for stratigraphic position). Note the repeated and predictable facies stacking pattern, with individual very thin beds of F1 and F2 that stack to form basin-floor mudstone bedsets (FA7), vertically separated by massive mudstones of F3 with common ash-rich sandstones (F12) to form massive mudstone packages (FA9). (B) Close-up view of an isolated very thin bed of F2 within FA9 dominated by F3 (196.32 m). Note the millimetre-scale pyrite nodules. (C) Close-up view of FA9 dominated by F3 with a carbonate cemented *Planolites* burrow (197.28 m). (D) Close-up view of a bioturbated vertical transition from FA7 dominated by F1 and F2, to darker and more bioturbated FA9 dominated by F3 (198.23 m). (E) Close-up view of FA7 dominated by F1 (198.60 m). Ch = Chondrites, He = Helminthopsis, Ph = Phycosiphon, Pl = Planolites
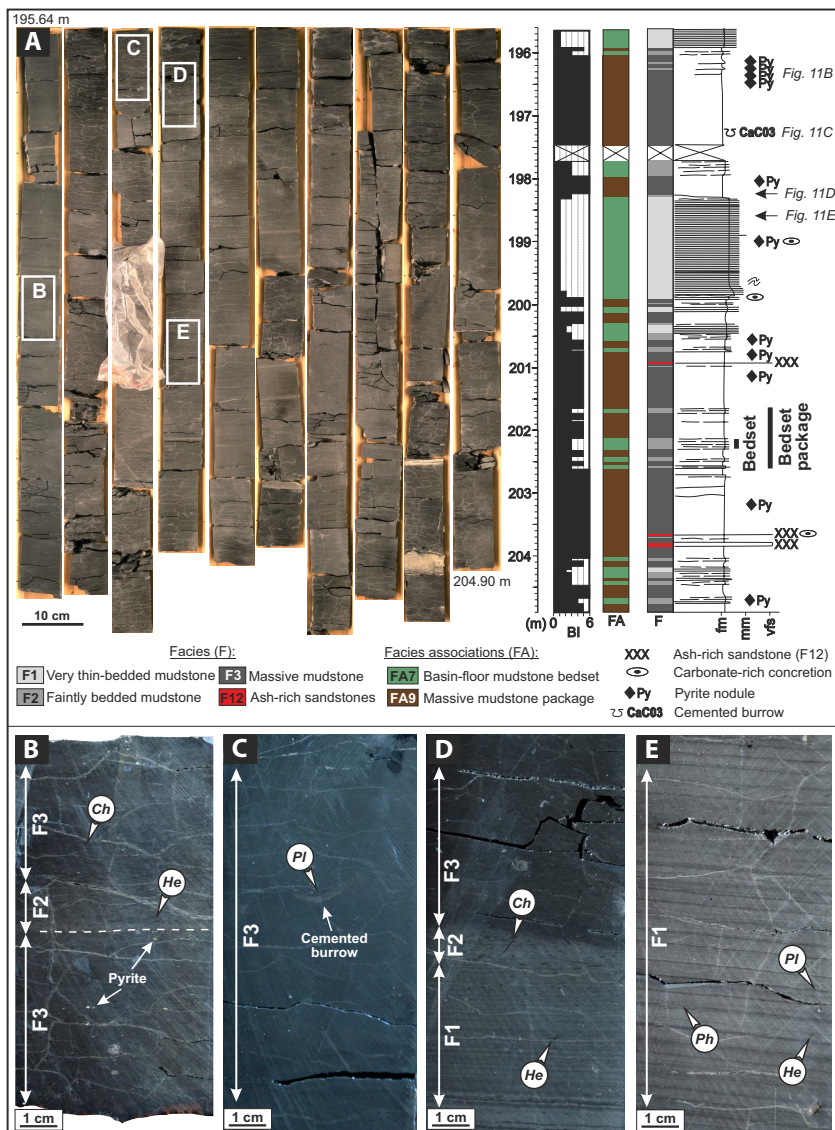
From core logging, the basin-floor mudstone units (Vischkuil-A, A5-A6, A-B) are dominantly composed of massive mudstone (F3; 45%) and very thin-bedded mudstone (F1; 31%), associated with minor faintly bedded mudstone (F2; 13%), interbedded sandstone and mudstone (F7; 5%), ash-rich sandstone (F12; 3%), structured sandstone (F5; 2%) and hybrid event bed (F8; 1%) (Figure 13; Table 1). Within the analysed thin sections of F1 in the basin-floor mudstones (see locations in Figure 9), the most common bed type identified is graded laminated (Bed type D; 39%), followed by normally graded (Bed type A; 26%), bioturbated (Bed type F; 24%), inversely to normally graded (Bed type C; 7.6%), bipartite (Bed type E; 3%) and inversely graded (Bed type B; 0.4%) (Figure 13).

In the core dataset, the basin-floor mudstones stack with a repeated alternation of bedsets (sensu Campbell, 1967) composed of F1, F2 and F7 (FA7; Table 2), and massive packages dominated by F3 (FA9; Table 2). This pattern occurs at two scales (Figures 9 and 11A):

(i) At the smallest scale (0.01–2 m), bedsets (FA7) are 0.01–1.70 m thick, and are vertically separated by relatively thin massive packages (FA9; <0.5 m thick), which are locally associated with ash-rich sandstones (F12), and isolated beds of F1, F2 and F7. Contacts between the bedsets (FA7) and the massive packages (FA9) are commonly sharp (Figure 11D).

(ii) At a larger scale (2–5 m), one or more bedsets (FA7), individually separated by relatively thin massive packages (FA9; <0.5 m thick), form bedset packages. Successive bedsets (FA7) within a bedset package can together form fining and thinning-upwards, coarsening and thickening-upwards, or coarsening and thickening-upward followed by fining and thinning-upward packages, or can be characterised by a more disorganised stacking pattern (Figures 9 and 11A). These bedset packages are vertically separated by thicker massive packages (FA9; >0.5 m thick), commonly associated with ash-rich sandstone (F12) (Figures 9 and 11A).
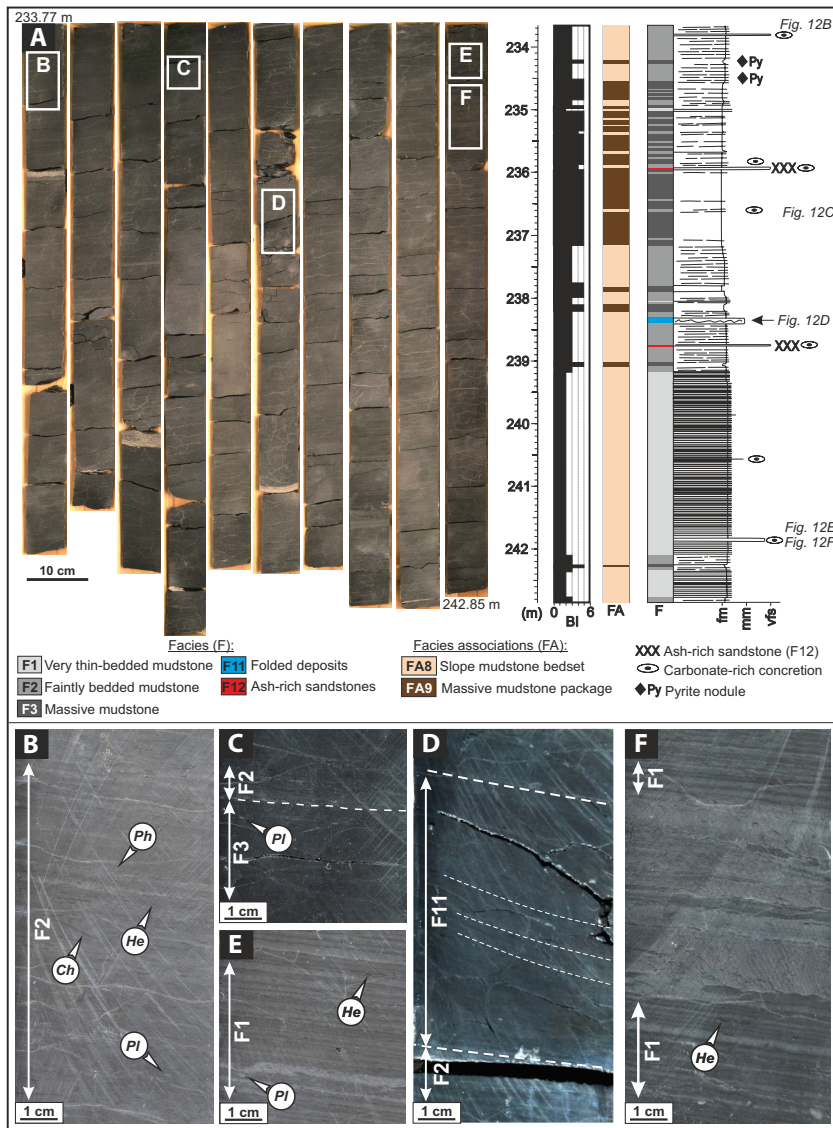
FIGURE 12 (A) Representative 9.08 m thick core section and sedimentological log from the lower slope B-C mudstone unit (BAV 1A; see Figure 10 for stratigraphic position). F1 and F2 stack to form slope mudstone bedsets (FA8) up to 8 m thick, intercalated with packages dominated by F3 to form massive mudstone packages (FA9). (B) Close-up view of FA8 dominated by F2 (233.80 m). (C) Close-up view of an isolated very thin bed of F2 within FA9 (236.60 m). (D) Close-up view of FA8 with folded deposits (F11) characterised by discordant beds (238.50 m). (E) Close up view of FA8 dominated by F1 beds, which are usually more bioturbated in the slope mudstones than in the basin-floor mudstones (241.70 m). (F) Close-up view of a carbonate-rich concretion within FA9 surrounded by F1 (241.90 m). Ch = Chondrites, he = Helminthopsis, Ph = Phycosiphon, Pl = Planolites

Facies proportions, nature of contact with bounding sandstone-prone units, and noticeable features are summarised below for the three basin-floor mudstone units.

5.1.1 | Vischkuil-A mudstone

The Vischkuil-A mudstone (7.3 m thick in BAV 1B) sharply overlies remobilised, mass-transport deposits (FA8; Table 2) of the Vischkuil Formation, and is sharply overlain by lobe axis deposits (FA1) of Unit A of the Laingsburg Formation (Figure 9B). This mudstone unit exhibits soft-sediment deformation and is dominated by F1 (38%) and F3 (29%), associated with F7 (13%), F2 (9%), F12 (6%) and F5 (5%) (Figures 9B and 13). The unit is also characterised by intercalated lobe fringe deposits (FA1) <50 cm thick (Figure 9B).

5.1.2 | A5-A6 mudstone

The A5-A6 mudstone (12.15 m thick in BAV 1B) sharply overlies lobe distal fringe deposits (FA2; Table 2) of Sub-unit A5 (after Sixsmith et al., 2004), and is sharply overlain by lobe fringe deposits (FA1) of Sub-unit A6 (Figure 9C). This mudstone unit is dominated by F3 (68%), associated with minor F1 (14%), F2 (14%), F7 (1%), F5 (1%), F8 (1%) and F12 (1%) (Figures 9C and 13).

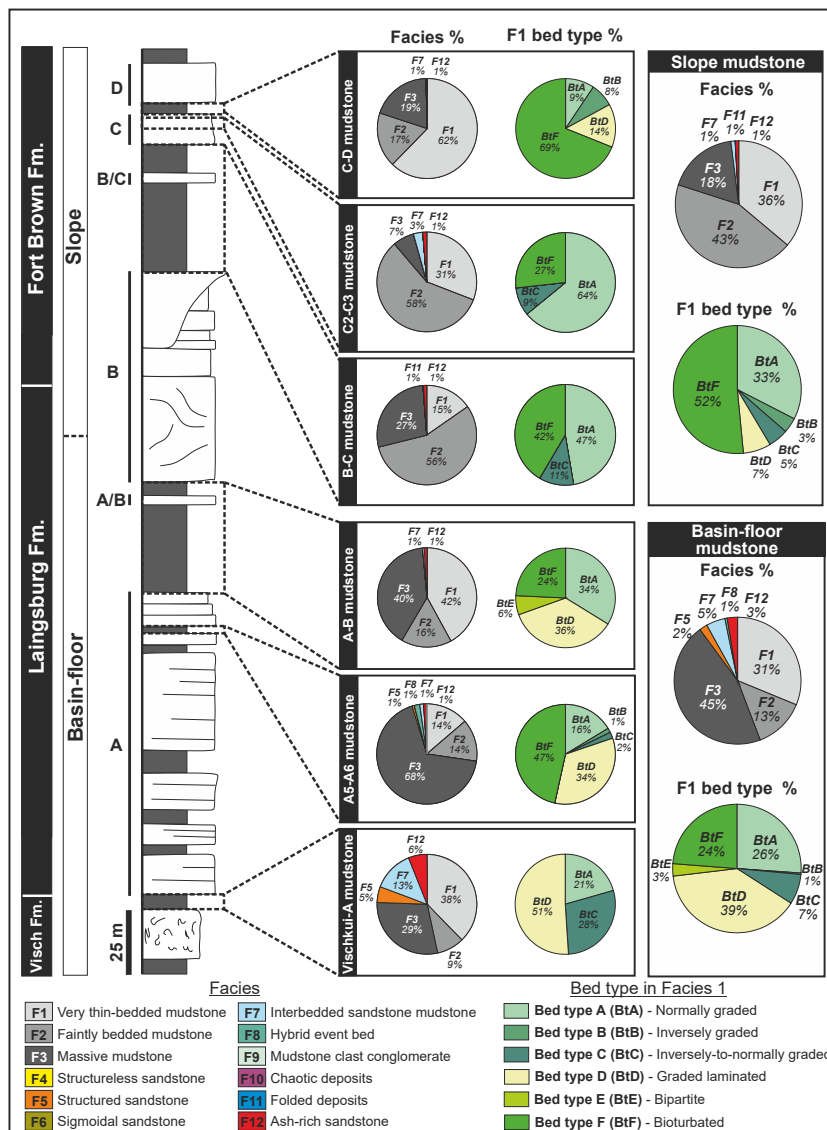### 5.1.3 | A-B mudstone

The A-B mudstone (39.7 m thick in BAV 1B) sharply overlies lobe distal fringe deposits (FA2; Table 2) of Unit A, and it is sharply overlain by lobe off-axis deposits

FIGURE 13 Stratigraphic distribution of facies and the six different types of bed identified in Facies 1 per mudstone unit (relative proportion by thickness)

(FA1) of Unit B (Figure 9D). This unit is dominated by F1 (42%) and F3 (40%), with minor associated F2 (16%), F12 (1%) and F7 (1%) (Figures 9D and 13). The A-B mudstone is also characterised by the presence of carbonate-rich concretions (Figure 9). A 5.10 m thick sandstone-prone package is intercalated in the succession (Unit A/B), bound by sharp contacts above and below, and is interpreted as disconnected basin-floor lobe deposits (Brooks et al., 2018a). The A-B mudstone unit shows a relatively constant basinward thinning towards the east-northeast (i.e. from 50 to 5 m), associated with a wedge-shape geometry (Figure 14B).

5.2 | Slope mudstones

Unit B of the Laingsburg Formation consists of weakly confined channel complexes and extensive levees

(to the west), interpreted as a base-of-slope succession, and mapped for 25 km basinward (to the east) into basin-floor lobe complexes (Brunt, et al., 2013b). Therefore, the overlying B-C mudstone is interpreted as a lower slope succession. It also contains a thin sandstone-prone package (Unit B/C), interpreted by Brooks et al. (2018a) as an intraslope lobe, deposited on a topographic step. However, this package is not encountered in the subsurface dataset reported here because of erosional removal by Unit C (Figure 10A). Unit C comprises channel-levee complexes (Hodgson et al., 2011; Morris et al., 2016) typical of a slope setting, and has been mapped for 80 km down depositional dip into basin-floor lobe complexes (Di Celma et al., 2011; Van der Merwe et al., 2014). Unit D includes deeply incised slope valley-fills, indicative of a mid-slope setting (Hodgson et al., 2011; Morris et al., 2016), with a basin-floor fan complex developed
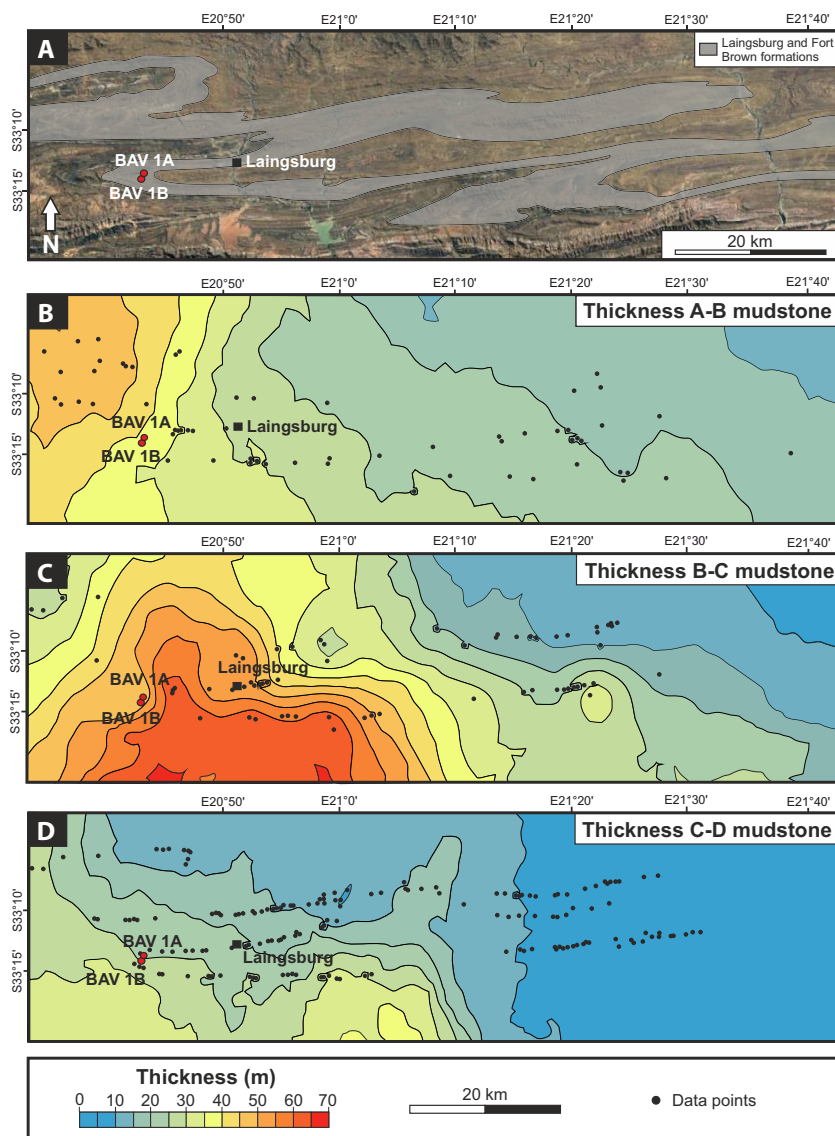
FIGURE 14 (A) Satellite view of the Laingsburg depocentre with drilling location of the two cores described in this study (BAV 1A and BAV 1B) and the outcrop belt of the Laingsburg and Fort Brown formations. (B) Thickness map of the A-B mudstone unit (basin-floor to base-of-slope). (C) Thickness map of the B-C mudstone unit (lower slope). (D) Thickness map of the C-D mudstone unit (mid slope). Note the overall gradual basinward thinning to the north-east and the resulting wedge shape geometry of each mudstone unit

70–100 km down depositional dip (Van der Merwe et al., 2014). This well-constrained palaeogeographical and stratigraphic context allows for confident interpretation of the C2-C3 and C-D mudstone units as mid slope deposits.

From core logging, the most dominant facies in the slope mudstone units (B-C, C2-C3, C-D) are faintly bedded mudstone (F2; 43%) and very thin-bedded mudstone (F1; 36%), associated with minor massive mudstones (F3; 18%), interbedded sandstone and mudstone (F7; 1%), folded deposits (F11; 1%), and ash-rich sandstones (F12; 1%) (Figures 10 and 13; Table 1). The most common bed type identified within the thin sections of F1 in slope mudstones (see locations in Figure 10) is bioturbated (Bed type F; 52%), followed by normally graded (Bed type A; 33%), graded laminated (Bed type D; 7%), inversely to normally graded (Bed type C; 5%), inversely graded (Bed type B; 3%) (Figure 13). Bipartite beds

(Bed type E) have not been observed in the thin-section dataset.

Similar to basin-floor deposits, slope mudstones consist of a repeated alternation of bedsets composed of F1, F2 and F7 (FA8; Table 2) and massive packages dominated by F3 (FA9; Table 2) (Figures 10 and 12A). However, the distinctive and predictable two-scale organisation recognised for the basin-floor mudstones (i.e. bedsets and bedset packages) is not observed in the slope deposits. Slope bedsets (FA8) are usually thicker (0.01–8 m thick), more bioturbated, and more commonly associated with carbonate-rich concretions when compared to basin-floor bedsets (Figures 10 and 12A). The massive mudstone packages (FA9) are 0.02–1.4 m thick (Figures 10 and 12). Facies proportions, nature of contacts with bounding sandstone-prone units, and noticeable features are summarised below for the three slope mudstone units.

5.2.1 | B-C mudstone

The B-C mudstone (49.3 m thick in BAV 1A) gradationally overlies Unit B external levee deposits (FA5; Table 2), and is truncated by slope valley-fill deposits (FA4) of Unit C (Figure 10A). This unit is dominated by F2 (56%) and F3 (27%), associated with minor F1 (15%), F12 (1%) and F11 (1%) (Figures 10A and 13). The B-C mudstone unit displays a thinning pattern towards the north, north-east and east (i.e. from 65 to 5 m), associated with a more radial wedge-shape geometry (Figure 14C).

5.2.2 | C2-C3 mudstone

The C2-C3 mudstone (7.7 m thick in BAV 1A) gradationally overlies external levee deposits (FA5; Table 2) of Sub-unit C2, and is gradationally overlain by frontal lobe deposits (FA7) of Sub-unit C3 (Morris et al., 2014b, 2016; Figure 10B). This unit is dominated by F2 (58%) and F1 (31%), associated with minor F3 (7%), F7 (3%) and F12 (1%) (Figures 10B and 13).

5.2.3 | C-D mudstone

The C-D mudstone (22.6 m thick in BAV 1A) sharply overlies frontal lobe deposits (FA7; Table 2) of Sub-Unit C3, and it is sharply overlain by external levee deposits (FA5) of Unit D (Kane & Hodgson, 2011; Figure 10C). This unit is dominated by F1 (62%), with minor associated F3 (19%), F2 (17%), F7 (1%) and F12 (1%) (Figures 10C and 13). The C-D mudstone unit exhibits a relatively constant basinward thinning towards the north-east (i.e. from 30 to 5 m), forming a wedge-shape geometry (Figure 14D).

6 | DISCUSSION

6.1 | What do basin-floor and slope mudstones represent?

Although at a regional scale (tens to hundreds of kilometres), the geometry of basin-margin clinothems vary spatially and temporally (Steventon et al., 2020), they are characterised by limited along-margin thickness changes compared to their basinward tapering wedge geometry, from foreset (slope) to bottomset (basin-floor). Controls on clinothem geometry include the location of sediment source(s) and the complex shelf process regimes, such as the interaction of reworking by tidal and wave processes, diffusion, and slope remobilisation and bypass (Nittrouer

et al., 1986). The description of the one-dimensional core dataset (Figures 9 and 10) combined with regional thickness mapping from continuous outcrop (Figure 14), and the three-dimensional contextual knowledge from previous studies of the Laingsburg succession, allow for a palaeogeographical reconstruction of the depositional environments recorded by the deep-water regional mudstone units (Figure 15). This permits investigation of the up-dip controls on slope and basin-floor mudstones.

6.1.1 | Basin-floor mudstones

Physical mapping across the Laingsburg depocentre has shown that the regional basin-floor mudstone units (Vischkuil-A, A5-A6, A-B) do not correlate laterally to coeval sandstones (Brunt, Hodgson, et al., 2013b; Sixsmith et al., 2004; Van der Merwe et al., 2014). The thickness map displays a basinward wedge-shape tapering geometry to the north-east and relatively constant lateral (across depositional strike) thicknesses (Figure 14B). This regional-scale architecture suggests that basin-floor mudstone units are the distal bottomset part of basin margin-scale clinothems, associated with a laterally extensive supply of mud beyond the shelf edge when deltas were situated in the inner shelf (Poyatos-Moré et al., 2019; Prather et al., 2017; Reading & Richards, 1994). Numerical stratigraphic models of delta-scale clinoforms combine advection and diffusion process to simulate across-margin and along-margin sediment transport and deposition (Driscoll & Karner, 1999; Pirmez et al., 1998). Similarly, in low-energy submarine slope and basin-floor environments, along-margin transport (Thiéblemont et al., 2019) combined with laterally extensive supply over the shelf-edge rollover (Poyatos-More et al., 2016), will result in basin-margin clinothems that change thickness basinward more abruptly than along-margin.

The basin-floor mudstones from the Laingsburg depocentre in the specific borehole locality stack in a repeated and predictable facies organisation, which occurs at two scales: (1) relatively thin massive packages dominated by debrites (FA9; <0.5 m thick) separate bedsets 0.01–1.70 m thick dominated by low-density turbidites (FA7); (2) thicker massive packages (FA9; >0.5 m thick) separate a group of bedsets to form bedset packages 2–5 m thick (Figures 9 and 11; Table 2). The well-ordered nature of the succession in the one-dimensional core dataset suggests both a laterally extensive supply of mud to form the wedge shape geometry of the units, and local feeder systems that delivered fine-grained sediment to the basin-floor.

The coeval up-dip shelf and slope deposits to the basin-floor mudstone units to the west and south-west of the study area are not preserved due to later uplift
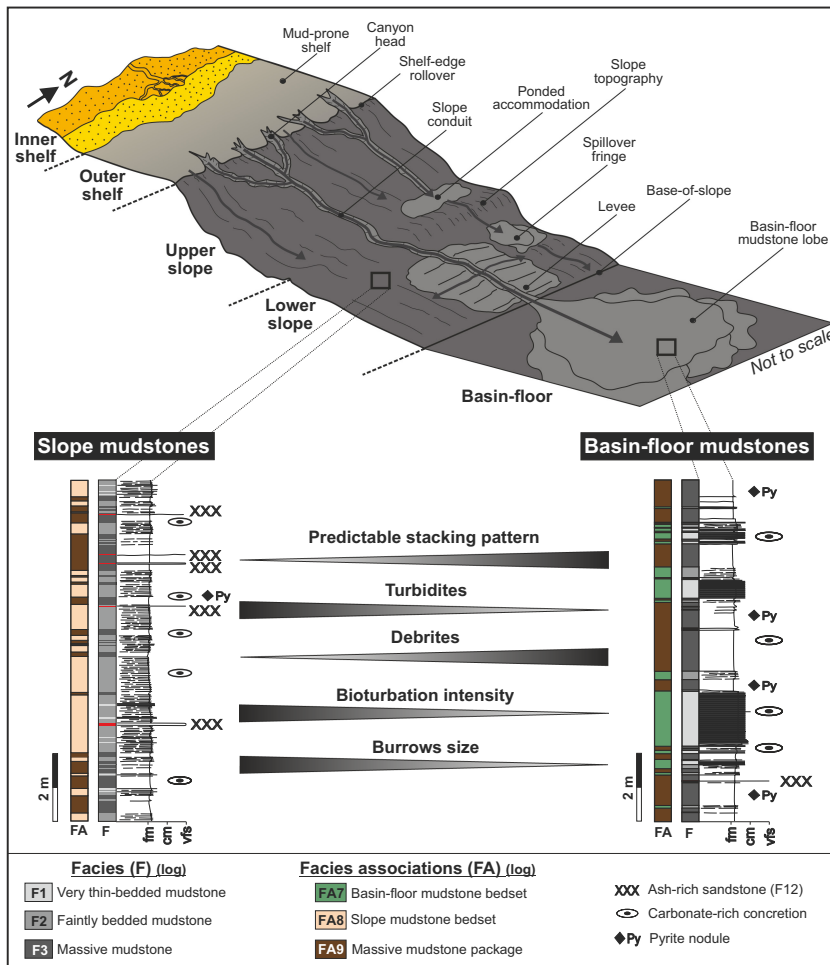
FIGURE 15 Reconstruction of shelf, slope and basin-floor depositional environments during accumulation of the regional deep-water mudstone units of the Laingsburg and Fort Brown formations. Representative core sections for slope (BAV 1A; 215 to 210 m) and basin-floor mudstones (BAV 1B; 202.5–192.5 m) are presented. Each mudstone unit has been mapped for >50 km down depositional dip and for >25 km across strike to confirm almost no sand deposited in the slope and basin floor at these times. The coeval high-accommodation shelf was mud-prone, and sediment gravity flows delivered mud to the slope and basin-floor by a combination of (a) laterally extensive supply beyond the shelf edge, and (b) point-sourced delivery through local slope canyon-channel systems, which were not completely filled and still active during backstepping of the sand-rich delivery systems

and erosion; therefore, the physiography of the sediment feeder systems is unknown. However, Units A and B of the Laingsburg Formation consist of base-of-slope to basin-floor sand-prone lobes, interpreted to be point sourced from a long-term fixed slope canyon system directly up depositional dip to the west-southwest of the study area (Brunt et al., 2013b; Grecula et al., 2003a). Local sea floor topography was produced on the basin-floor to base-of-slope regions during the accumulation of the mudstone units (Brooks et al., 2018a). Thus, the inferred presence of sea floor topography and long-term slope conduits directly up depositional dip of the study area suggest that mud, in the specific borehole locality, may have also been sourced from: i) flows stripped from intraslope or basin-floor confinement to build spillover fringes on the basin-floor (Brooks et al., 2018b; Sinclair & Tomasso, 2002), with some potential sand being trapped up depositional dip (intraslope lobes; Plink-Björklund & Steel, 2002; Spychala et al., 2015); and/or (ii) flows delivered through partially filled submarine slope conduits to build basin-floor mudstone lobes (Boulesteix et al., 2020). Spillover fringe deposits originate from the uppermost dilute part of flows breaching up-dip topography (Sinclair & Tomasso, 2002), and

therefore, only waning, low-density turbidity currents are expected to be deposited in the downdip environments (Brooks et al., 2018b). However, microscope observations suggest the basin-floor mudstone bedsets (FA7) accumulated from a wide range of sediment gravity flows, mostly low-density turbidity currents (Figures 3 and 13), with evidence of flow fluctuations (Bed type D; Figure 3D). Also, the low to high degree of bioturbation (BI: 1–4) of the basin-floor mudstone bedsets (FA7) points towards variably stressed sea floor conditions, potentially linked to periods of more frequent and efficient sediment gravity flows reaching the basin-floor and/or variations of the geochemistry of bottom waters and porewaters (Heard & Pickering, 2008; Wetzel, 1984). The variable vertical stacking pattern of successive bedsets (FA7; Figure 9) separated by thin massive mudstones (FA9; <0.5 m thick) may also suggest compensational stacking (Boulesteix et al., 2020; Prélat et al., 2009; Prélat & Hodgson, 2013). The well-ordered and potentially compensational nature, the sedimentological evidence for flow fluctuations, and the ichnological evidence for frequent sediment delivery to the basin-floor, support an interpretation of the mudstone bedsets (FA7) as basin-floor mudstone lobes

(Figure 15), supplied via underfilled slope canyons. The higher bioturbation intensity (BI: 5–6) associated with the massive mudstone packages (FA9) suggests more favourable physico-chemical conditions for burrowing organisms, linked to less frequent debris flows reaching the basin-floor (Heard & Pickering, 2008; Wetzel, 1984). The debrite-rich packages (FA9) are therefore interpreted as accumulated outside the mudstone lobes, potentially linked to autogenic compensational stacking and/or allogenically-controlled backstepping of the sediment delivery system (Boulesteix et al., 2019, 2020). The relatively thick massive mudstone packages (FA9; >0.5 m thick) are more commonly associated with ash-rich sandstones (F12; Table 1), which suggests longer-term decrease of sedimentation rate on the basin-floor.

The relatively high proportion of debrites (F3: 45%; Figure 13) in the basin-floor mudstones is consistent with a distal position, more prone to flow transformations from turbulent to laminar (Baker & Baas, 2020; Haughton et al., 2003; Hodgson, 2009; Kane et al., 2017; Talling et al., 2004). The high mud content on the sea floor during the interpreted relative sea-level highstand periods in the Karoo Basin (Flint et al., 2011) and its incorporation in sediment gravity-flows may have favoured flow transformations by enhancing the damping of flow turbulence (Baas et al., 2011; Baas & Best, 2002). Deep-water massive mudstones are commonly interpreted as hemipelagites based on their homogeneous texture in cores and outcrops. However, this study, along with other recent studies of deep-water mudstones (Boulesteix et al., 2019, 2020; Emmings et al., 2020; Könitzer et al., 2014; Newport et al., 2018) indicate that massive-looking mudstones at macroscopic scale may contain microscopic outsized particles, which suggest they are often deposited by much higher energy processes than previously assumed.

6.1.2 | Slope mudstones

Similar to the basin-floor deposits, the slope mudstone units (B-C, C2-C3, C-D) do not correlate laterally to any coeval sandstones, and show a basinward wedge-shape tapering geometry and relatively constant lateral thicknesses (Figure 14C,D). This suggests they also form part of basin margin clinothems (i.e. foresets), associated with a laterally extensive supply of mud beyond the shelf edge when deltas were shelf-confined (Poyatos-Moré et al., 2019; Prather et al., 2017; Reading & Richards, 1994). However, in contrast to the basin-floor mudstones, the slope deposits show: (i) a higher proportion of low-density turbidites (82% in the slope versus 55% in the basin-floor) compared to debrites (18% in the slope versus 45% in the basin-floor);

(ii) a less predictable stacking pattern; (iii) more common carbonate-rich concretions and carbonate-cemented burrows; (iv) higher bioturbation intensity; and v) larger burrows (Figures 10, 12 and 13). Units C and D of the Fort Brown Formation consist of channel-levee systems in a submarine slope setting in the Baviaans area (Di Celma et al., 2011; Hodgson et al., 2011; Morris et al., 2016), with evidence for a stepped profile (Brooks et al., 2018a; Van der Merwe et al., 2014). The composite erosion surface of a Unit D slope valley remained underfilled during the abandonment phase (Hodgson et al., 2011; Morris et al., 2016), which suggests slope conduits may have remained partially open and active during the accumulation of the intercalated regional mudstone units. Sea floor topography was generated on the slope during the accumulation of mudstones, producing steeper segments, which may have influenced sediment gravity flows (Brooks et al., 2018a). Slope mudstone bedsets (FA8; Table 2) may therefore locally represent spillover fringe deposits (Figure 15) (Brooks et al., 2018b; Sinclair & Tomasso, 2002), with some sand-prone parts of flows being trapped up depositional dip to form intraslope lobes (Plink-Björklund & Steel, 2002; Spychala et al., 2015). However, slope bedsets (FA8) may also be derived from flows escaping lateral confinement from slope conduits to build external levees (Figure 15) (Beaubouef, 2004; Buffington, 1952; Kane & Hodgson, 2011; Normark et al., 1980). The aggradational stacking of FA8 deposits, with packages up to 8 m thick (Figures 10 and 12), may be also explained by local flow confinement in slope accommodation (Ferry et al., 2005; Spychala et al., 2015, 2017). The less predictable stacking pattern of the slope mudstones in the one-dimensional core dataset (Figure 10), and the three-dimensional palaeogeographical control, suggest that mud may have accumulated by a combination of processes along a topographically complex slope, and in a wider range of depositional sub-environments compared to the basin-floor (Figure 15).

The higher proportion of low-density turbidites in the slope mudstones (82%) compared to the basin-floor mudstones (55%) may be explained by the more proximal position relative to the shelf edge, with more common low-density turbidity currents reaching this part of the margin profile. The higher bioturbation intensity, larger burrows and more common carbonate-rich concretions of FA8 deposits (slope bedsets) compared to FA7 (basin-floor bedsets) are consistent with periods of slower sediment accumulation of the FA8 deposits, which may be explained by a lateral position relative to slope conduits. The strong bioturbation of the intercalated massive mudstone packages (FA9; Table 2) suggests they accumulated from more infrequent debris flows (Heard & Pickering, 2008; Wetzel, 1984), and are interpreted to represent periods of

significantly reduced sediment input, potentially linked to allogenic and/or autogenic backstepping or avulsion of the sediment delivery system (Boulesteix et al., 2019).

6.2 | Implications for the delivery of mud to deep-water environments

The Laingsburg deep-water succession exhibits an organised alternation of sandstone-prone and mudstone-prone units (Figure 1C). This stratigraphic motif has been commonly observed in other deep-water successions in outcrops (Gardner et al., 2003; Grundvåg et al., 2014; Hodgson et al., 2006; Mutti & Normark, 1987; Pickering & Cantalejo, 2015; Pyles, 2008; Terlaky et al., 2016), and in subsurface datasets (Beaubouef & Friedmann, 2000; Gervais et al., 2006; Prather et al., 2017; Sweet et al., 2019; Sylvester et al., 2012; Wynn et al., 2000). In the Laingsburg depocentre, the sandstone-prone deep-water units have been interpreted to be lowstand systems tracts, when deltas reached the shelf edge, or when the shelf was exposed, supplying sand directly to the heads of submarine canyon-channel systems (Flint et al., 2011). The regional mudstone units investigated in this study (Vischkuil-A, A5-A6, A-B, B-C, C2-C3, C-D) have been interpreted to be combined transgressive and highstand systems tracts, deposited during relative sea-level rise and highstand, when deltas were shelf-confined, resulting in deactivation of slope canyon-channel systems and cessation of sand supply to deep-water environments (Flint et al., 2011). Commonly, deep-water regional mudstones are interpreted to be dominated by hemipelagic fallout deposits, passively draping the sea floor (Flint et al., 2011; Posamentier & Kolla, 2003; Posamentier & Walker, 2006; Pyles, 2008). However, this study challenges this paradigm, and shows that: (i) mud can be delivered to the slope and the basin-floor by a combination of laterally extensive supply, and point-source delivery systems; and (ii) deep-water mudstones can be dominated by the product of multiple sediment gravity flows, including a wide range of low-density turbidity currents and low-strength cohesive debris flows (Figure 15).

Several physical processes must be considered to explain the relatively continuous transfer of mud to the shelf edge and the heads of shelf-incised slope conduits during the absence of the sand-dominated systems. Monitoring programs of modern shelf environments have revealed that mud can be transported by energetic processes, such as hyperpycnal flows, and resuspension of mud by waves and storms, generating turbulent transport of fluid mud that migrates either along, or across the shelf (Cacchione et al., 1995; Kineke et al., 1996; Ogston et al., 2000; Traykovski et al., 2000; Wright et al., 2001). Some of this mud may be stored on the shelf to form mud belts (Lee & Chu, 2001; Wells &

Coleman, 1981). Mud can also be efficiently advected to the shelf edge and the canyon heads, and transferred down the slope through canyon-channel systems (Bourrin et al., 2015; Palanques et al., 2006; Puig et al., 2003; Walsh & Nittrouer, 1999). The coeval shelf of the deep-water succession investigated here is now absent because of later uplift and erosion, and therefore, the sedimentary processes that were acting on the shelf up depositional dip are unknown. However, the overlying shelf succession of the Waterford Formation shows evidence for recurrent supply of mud to the shelf edge and the upper slope, mainly through the action of wave and/or storm reworking of mud previously deposited from river floods (Poyatos-Moré et al., 2016). This suggests that similar processes may have acted on the coeval shelf to the Laingsburg and Fort Brown formations, during high accommodation times, to efficiently transfer mud beyond the shelf edge and to the head of underfilled slope canyons. The basinward wedge-shape tapering geometry of the mudstone units at regional scale suggests that most of the mud was transported and deposited on the slope and in proximal basin-floor environments by recurrent gravity-driven supply from a laterally extensive supply (Figure 15). However, the sedimentological and stratigraphic evidence for the accumulation of point-sourced basin-floor mudstone lobes also suggest that slope conduits were not necessarily deactivated during the backstepping or avulsion of the sand-dominated part of the system, and could deliver mud to some parts of the basin-floor (Figure 15). These findings have important implications for the correct interpretation of deep-water mudstone depositional processes, and indicate that significant energetic processes can still occur in deep-water systems during periods when sand is stored on the shelf.

7 | CONCLUSION

Analysis of two cores from research boreholes tied to regionally continuous outcrops and a well-constrained three-dimensional stratigraphic and palaeogeographical context established from previous studies has allowed the variability in depositional processes and stacking patterns between slope and basin-floor mudstones to be documented within the same basin margin succession (Laingsburg depocentre, Karoo Basin, South Africa). Traditionally, deep-water mudstones are interpreted as dominated by the product of hemipelagic fallout, but the mudstones from the Laingsburg depocentre are heterogeneous and dominated by sediment gravity flow deposits. In the one-dimensional core dataset, basin-floor mudstones exhibit a repeated alternation of bedsets and massive packages. Microscopic observations indicate bedsets consist of six bed types deposited by a wide range of low-density turbidity currents

(waning, waxing, waxing-to-waning, multi-pulsed), and occasional transitional flows. The intercalated massive mudstones are pervasively bioturbated, contain outsized sand particles, and are interpreted as being deposited by low-strength cohesive debris flows, with evidence of flow transformations from turbulent to laminar. The slope mudstones show a similar facies assemblage, but are characterised by a higher proportion of low-density turbidites (82% in the slope versus 55% in the basin-floor) compared to debrites (18% in the slope versus 45% in the basin-floor), a less predictable facies stacking pattern, more common carbonate-rich concretions, a higher bioturbation intensity, and larger burrows; the last three being the result of periods of lower sedimentation rate. The thickness maps of the mudstone units across the 2500 km^2 study area show a basinward wedge-shape tapering geometry but rather uniform along margin thickness changes. These geometries are consistent with forming the distal part of basin margin clinothems, and thus a laterally extensive source of mud supply beyond the shelf edge when deltas were situated in the inner shelf combined with along-margin transport processes. However, the stratigraphic context, as well as the well-ordered and repeated organisation of the basin-floor mudstones in the core locality, suggest that some of the mud was locally point-sourced through underfilled slope conduits, associated with relative sea-level change, and autogenic compensational stacking of basin-floor mudstone lobes. The less predictive stacking pattern of the slope mudstones suggests they probably accumulated in a wider range of depositional environments within a topographically complex slope (i.e. ponded accommodation, minor gully/channel-fills, levees). The development of recognition criteria to distinguish between slope and basin-floor mudstones has implications for the palaeogeographical interpretations of other deep-water mudstone successions. The wide spectrum of depositional processes and environments recognised within these deep-water mudstones suggest that mud-rich submarine canyon-channel systems can still remain as pathways to deliver recurrent sediment gravity flows to the slope and basin-floor during times when sand is sequestered on the shelf. This study shows that flow energy conditions in deep-water mud-prone environments can be significantly higher than previously assumed, and may provide insights to improve models for the transport and deposition of fine-grained particles, such as microplastics and other pollutants in the deep oceans.

CONFLICT OF INTEREST

The authors have no conflict of interest to declare.

DATA AVAILABILITY STATEMENT

The data that support the findings of this study are available from the corresponding author upon reasonable request.

ORCID

Kévin Boulesteix https://orcid.org/0000-0002-3349-2609
Miquel Poyatos-Moré https://orcid.org/0000-0001-7813-8868
Stephen S. Flint https://orcid.org/0000-0002-0558-6261
David M. Hodgson https://orcid.org/0000-0003-3711-635X
Kevin T. Taylor https://orcid.org/0000-0001-7024-5001
Rufus L. Brunt https://orcid.org/0000-0002-3276-3147

REFERENCES

Allen, J.R.L. (1982) *Sedimentary structures: their character and physical basis*, volumes *1*, 2: Amsterdam, Elsevier, 593p, 663 p.

Arnott, R.W.C. & Hand, B.M. (1989) Bedforms, primary structures and grain fabric in the presence of suspended sediment rain. *Journal of Sedimentary Research*, *59*(6), 1062–1069.

Baas, J.H. & Best, J.L. (2002) Turbulence modulation in clay-rich sediment-laden flows and some implications for sediment deposition. *Journal of Sedimentary Research*, *72*(3), 336–340.

Baas, J.H., Best, J.L. & Peakall, J. (2011) Depositional processes, bedform development and hybrid bed formation in rapidly decelerated cohesive (mud-sand) sediment flows. *Sedimentology*, *58*(7), 1953–1987.

Baker, M.L. & Baas, J.H. (2020) Mixed sand–mud bedforms produced by transient turbulent flows in the fringe of submarine fans: indicators of flow transformation. *Sedimentology*, *67*, 2645–2671.

Beaubouef, R.T. (2004) Deep-water leveed-channel complexes of the Cerro Toro Formation, Upper Cretaceous, southern Chile. *AAPG Bulletin*, *88*(11), 1471–1500.

Beaubouef, R.T. & Friedmann, S.J. (2000) High resolution seismic/ sequence stratigraphic framework for the evolution of Pliocene intra slope basins, western Gulf of Mexico: depositional models and reservoir analogs. In: *GCSSEPM Foundation 20th Annual Research Conference Deep-Water Reservoirs of the Word*. Houston, Texas, December, 3–6, pp. 40–60.

Bennett, M.R., Doyle, P. & Mather, A.E. (1996) Dropstones: their origin and significance. *Palaeogeography, Palaeoclimatology, Palaeoecology*, *121*(3–4), 331–339.

Best, J.L. & Bridge, J. (1992) The morphology and dynamics of low amplitude bedwaves upon upper stage plane beds and the preservation of planar laminae. *Sedimentology*, *39*(5), 737–752.

Blewett, S. & Phillips, D. (2016) An overview of Cape Fold Belt geochronology: implications for sediment provenance and the timing of orogenesis. In: Linol, B. & De Wit, M.J. (Eds.) *Origin and evolution of the Cape Mountains and Karoo Basin*. Cham: Springer, pp. 45–55.

Boulesteix, K., Poyatos-Moré, M., Flint, S.S., Taylor, K.G., Hodgson, D.M. & Hasiotis, S.T. (2019) Transport and deposition of mud in deep-water environments: processes and stratigraphic implications. *Sedimentology*, 66(7), 2894–2925.

Boulesteix, K., Poyatos-Moré, M., Hodgson, D.M., Flint, S.S. & Taylor, K.G. (2020) Fringe or background: characterising deep-water mudstones beyond the basin-floor fan sandstone pinchout. *Journal of Sedimentary Research*, 90(12), 1678–1705.

Bourget, J., Ainsworth, R.B. & Thompson, S. (2014) Seismic stratigraphy and geomorphology of a tide or wave dominated shelf-edge delta (NW Australia): process-based classification from 3D seismic attributes and implications for the prediction of deep-water sands. *Marine and Petroleum Geology*, 57, 359–384.

Bourrin, F., Many, G., de Madron, X.D., Martín, J., Puig, P., Houpert, L., Testor, P., Kunesch, S., Mahiouz, K. & Béguery, L. (2015) Glider monitoring of shelf suspended particle dynamics and transport during storm and flooding conditions. *Continental Shelf Research*, 109, 135–149.

Brooks, H.L., Hodgson, D.M., Brunt, R.L., Peakall, J., Poyatos-Moré, M. & Flint, S.S. (2018a) Disconnected submarine lobes as a record of stepped slope evolution over multiple sea-level cycles. *Geosphere*, 14, 1753–1779.

Brooks, H.L., Hodgson, D.M., Brunt, R.L., Peakall, J., Hofstra, M. & Flint, S.S. (2018b) Deep-water channel-lobe transition zone dynamics: processes and depositional architecture, an example from the Karoo Basin, South Africa. *GSA Bulletin*, 130(9–10), 1723–1746.

Brunt, R.L., Di Celma, C.N., Hodgson, D.M., Flint, S.S., Kavanagh, J.P. & van der Merwe, W.C. (2013a) Driving a channel through a levee when the levee is high: an outcrop example of submarine downdip entrenchment. *Marine and Petroleum Geology*, 41, 134–145.

Brunt, R.L., Hodgson, D.M., Flint, S.S., Pringle, J.K., Di Celma, C., Prélat, A. & Grecula, M. (2013b) Confined to unconfined: anatomy of a base-of-slope succession, Karoo Basin, South Africa. *Marine and Petroleum Geology*, 41, 206–221.

Buffington, E.C. (1952) Submarine 'natural levees'. *Journal of Geology*, 60, 473–479.

Cacchione, D.A., Drake, D.E., Kayen, R.W., Sternberg, R.W., Kineke, G.C. & Tate, G.B. (1995) Measurements in the bottom boundary layer on the Amazon subaqueous delta. *Marine Geology*, 125(3–4), 235–257.

Campbell, C.V. (1967) Lamina, laminaset, bed and bedset. *Sedimentology*, 8(1), 7–26.

Carvajal, C. & Steel, R. (2009) Shelf-edge architecture and bypass of sand to deep-water: influence of shelf-edge processes, sea level, and sediment supply. *Journal of Sedimentary Research*, 79(9), 652–672.

Catuneanu, O., Hancox, P.J. & Rubidge, B.S. (1998) Reciprocal flexural behaviour and contrasting stratigraphies: a new basin development model for the Karoo retroarc foreland system, South Africa. *Basin Research*, 10, 417–439.

Chukwuma, K. & Bordy, E.M. (2016) Spatiotemporal sedimentary facies variations in the lower Permian Whitehill formation, Ecca group, Karoo Basin. In: Linol, B. & De Wit, M.J. (Eds.) *Origin and evolution of the Cape Mountains and Karoo Basin*. Cham: Springer, pp. 101–110.

Cosgrove, G.I.E., Hodgson, D.M., Poyatos-Moré, M., Mountney, N.P. & McCaffrey, W.D. (2018) Filter or conveyor? Establishing relationships between clinoform rollover trajectory, sedimentary process regime, and grain character within intrashelf clinoform, offshore New Jersey, U.S.A. *Journal of Sedimentary Research*, 88, 917–941.

Covault, J.A., Normark, W.R., Romans, B.W. & Graham, S.A. (2007) Highstand fans in the California borderland: the overlooked deep-water depositional systems. *Geology*, 35(9), 783–786.

De Wit, M.J. & Ransome, I.G.D. (1992) Regional inversion tectonics along the southern margin of Gondwana. In: De Wit, M.J. & Ransome, I.G.D. (Eds.) *Inversion tectonics of the cape Fold Belt, Karoo and cretaceous basins of southern Africa*. Rotterdam: A.A. Balkema, pp. 15–21.

Di Celma, C., Brunt, R.L., Hodgson, D.M., Flint, S.S. & Kavanagh, J.P. (2011) Spatial and temporal evolution of a Permian submarine slope channel–levee system, Karoo Basin, South Africa. *Journal of Sedimentary Research*, 81, 579–599.

Dixon, J.F., Steel, R.J. & Olariu, C. (2012) River-dominated, shelf-edge deltas: delivery of sand across the shelf break in the absence of slope incision. *Sedimentology*, 59, 1133–1157.

Driscoll, N.W. & Karner, G.D. (1999) Three-dimensional quantitative modeling of clinoform development. *Marine Geology*, 154, 383–398.

Emmings, J.F., Davies, S.J., Vane, C.H., Moss-Hayes, V. & Stephenson, M.H. (2020) From marine bands to hybrid flows: sedimentology of a Mississippian black shale. *Sedimentology*, 67(1), 261–304.

Ferry, J.N., Mulder, T., Parize, O. and Raillard, S. (2005) *Concept of equilibrium profile in deep-water turbidite system: effects of local physiographic changes on the nature of sedimentary process and the geometries of deposits*. In: Hodgson, D.M. and Flint, S.S. (Eds), Geological society, London, Special Publications, 244(1), pp. 181–193.

Figueiredo, J.J.P., Hodgson, D.M. & Flint, S.S. (2010) Depositional environments and sequence stratigraphy of an exhumed Permian mud-dominated submarine slope succession, Karoo basin, South Africa. *Journal of Sedimentary Research*, 80, 97–118.

Flint, S.S., Hodgson, D.M., Sprague, A.R., Brunt, R.L., Van der Merwe, W.C., Figueiredo, J., Prélat, A., Box, D., Di Celma, C. & Kavanagh, J.P. (2011) Depositional architecture and sequence stratigraphy of the Karoo Basin-floor to shelf edge succession, Laingsburg depocenter, South Africa. *Marine and Petroleum Geology*, 28, 658–674.

Fonnesu, M., Haughton, P., Felletti, F. & McCaffrey, W. (2015) Short length-scale variability of hybrid event beds and its applied significance. *Marine and Petroleum Geology*, 67, 583–603.

Fonnesu, M., Patacci, M., Haughton, P.D.W., Felletti, F. & McCaffrey, W.D. (2016) Hybrid event beds generated by local substrate delamination on a confined-basin floor. *Journal of Sedimentary Research*, 86, 929–943.

Gardner, M.H., Borer, J.M., Melick, J.J., Mavilla, N., Dechesne, M. & Wagerle, R.N. (2003) Stratigraphic process-response model for submarine channels and related features from studies of Permian brushy canyon outcrops, West Texas. *Marine and Petroleum Geology*, 20(6–8), 757–787.

Gervais, A., Savoye, B., Mulder, T. & Gonthier, E. (2006) Sandy modern turbidite lobes: a new insight from high resolution seismic data. *Marine and Petroleum Geology*, 23(4), 485–502.

Gingras, M.K., MacEachern, J.A. & Dashtgard, S.E. (2011) Process ichnology and the elucidation of physico-chemical stress. *Sedimentary Geology*, 237(3–4), 115–134.

Gong, C., Steel, R.J., Wang, Y., Lin, C. & Olariu, C. (2016) Grain size and transport regime at shelf edge as fundamental controls on delivery of shelf-edge sands to Deepwater. *Earth-Science Reviews*, 157, 32–60.

Gorsline, D.S. (1978) Anatomy of margin basins; presidential address. *Journal of Sedimentary Research*, 48(4), 1055–1068.

Grecula, M., Flint, S.S., Potts, G., Wickens, H.D.V. & Johnson, S. (2003a) Partial ponding of turbidite systems in a basin with subtle growth-fold stratigraphy: Laingsburg-Karoo, South Africa. *Journal of Sedimentary Research*, 73, 603–620.

Grecula, M., Flint, S.S., Wickens, H.D.V. & Johnson, S.D. (2003b) Upward-thickening patterns and lateral continuity of Permian sand-rich turbidite channel fills, Laingsburg Karoo, South Africa. *Sedimentology*, 50(5), 831–853.

Grundvåg, S.A., Johannessen, E.P., Helland-Hansen, W. & Plink-Björklund, P. (2014) Depositional architecture and evolution of progradationally stacked lobe complexes in the Eocene Central Basin of Spitsbergen. *Sedimentology*, 61(2), 535–569.

Hadler-Jacobsen, F., Johannessen, E.P., Ashton, N., Henriksen, S., Johnson, S.D. and Kristensen, J.B. (2005) Submarine fan morphology and lithology distribution: a predictable function of sediment delivery, gross shelf-to-basin relief, slope gradient and basin topography. In: Doré, A.G. and Vinin, B.A. (Eds) *Petroleum Geology: North-West Europe and Global Perspectives-Proceedings of the 6th Petroleum Geology Conference*, Geological Society, London. London: The Geological Society, pp. 1121–1145.

Haughton, P.D.W., Barker, S.P. & McCaffrey, W.D. (2003) Linked debrites in sand-rich turbidite systems-origin and significance. *Sedimentology*, 50(3), 459–482.

Heard, T.G. & Pickering, K.T. (2008) Trace fossils as diagnostic indicators of deep-marine environments, Middle Eocene Ainsa-Jaca basin, Spanish Pyrenees. *Sedimentology*, 55(4), 809–844.

Ho, V.L., Dorrell, R.M., Keevil, G.M., Burns, A.D. & McCaffrey, W.D. (2018) Pulse propagation in turbidity currents. *Sedimentology*, 65(2), 620–637.

Hodgson, D.M. (2009) Distribution and origin of hybrid beds in sand-rich submarine fans of the Tanqua depocentre, Karoo Basin, South Africa. *Marine and Petroleum Geology*, 26(10), 1940–1956.

Hodgson, D.M., Flint, S.S., Hodgetts, D., Drinkwater, N.J., Johannessen, E.P. & Luthi, S.M. (2006) Stratigraphic evolution of a fine-grained submarine fan systems, Tanqua Depocenter, Karoo Basin, South Africa. *Journal of Sedimentary Research*, 76(1), 20–40.

Hodgson, D.M., Di Celma, C., Brunt, R.L. & Flint, S.S. (2011) Submarine slope degradation and aggradation and the stratigraphic evolution of channel-levee systems. *Journal of the Geological Society*, 168, 625–628.

Hunter, R.E. (1977) Terminology of cross-stratified sedimentary layers and climbing-ripple structures. *Journal of Sedimentary Research*, 47(2), 697–706.

Iverson, R.M. (1997) The physics of debris flows. *Reviews of Geophysics*, 35, 245–296.

Jobe, Z.R., Lowe, D.R. & Morris, W.R. (2012) Climbing-ripple successions in turbidite systems: depositional environments, sedimentation rates and accumulation times. *Sedimentology*, 59(3), 867–898.

Johannessen, E.P. & Steel, R.J. (2005) Shelf-margin clinoforms and prediction of Deepwater sands. *Basin Research*, 17, 521–550.

Johnson, M.R., Van Vuuren, C.J., Hegenberger, W.F., Key, R. & Show, U. (1996) Stratigraphy of the Karoo Supergroup in southern Africa: an overview. *Journal of African Earth Sciences*, 23(1), 3–15.

Jones, G.E.D., Hodgson, D.M. & Flint, S.S. (2015) Lateral variability in clinoform trajectory, process regime, and sediment dispersal patterns beyond the shelf-edge rollover in exhumed basin margin-scale clinothems. *Basin Research*, 27, 657–680.

Jopling, A.V. & Walker, R.G. (1968) Morphology and origin of ripple-drift cross-lamination, with examples from the Pleistocene of Massachusetts. *Journal of Sedimentary Petrology*, 38(4), 971–984.

Kane, I.A. & Hodgson, D.M. (2011) Sedimentological criteria to differentiate submarine channel levee subenvironments: exhumed examples from the Rosario Fm. (upper cretaceous) of Baja California, Mexico, and the Fort Brown Fm. (Permian), Karoo basin, S. Africa. *Marine and Petroleum Geology*, 28(3), 807–823.

Kane, I.A. & Pontén, A.S.M. (2012) Submarine transitional flow deposits in the Paleogene Gulf of Mexico. *Geology*, 40(12), 1119–1122.

Kane, I.A., Pontén, A.S., Vangdal, B., Eggenhuisen, J.T., Hodgson, D.M. & Spychala, Y.T. (2017) The stratigraphic record and processes of turbidity current transformation across deep-marine lobes. *Sedimentology*, 64(5), 1236–1273.

Kineke, G.C., Sternberg, R.W., Trowbridge, J.H. & Geyer, W.R. (1996) Fluid-mud processes on the Amazon continental shelf. *Continental Shelf Research*, 16(5–6), 667–696.

Kneller, B.C. & Branney, M.J. (1995) Sustained high-density turbidity currents and the deposition of thick massive sands. *Sedimentology*, 42(4), 607–616.

Kneller, B. & McCaffrey, W.D. (2003) The interpretation of vertical sequences in turbidite beds: the influence of longitudinal flow structures. *Journal of Sedimentary Research*, 73, 706–713.

Könitzer, S.F., Davies, S.J., Stephenson, M.H. & Leng, M.J. (2014) Depositional controls on mudstone lithofacies in a basinal setting: implications for the delivery of sedimentary organic matter. *Journal of Sedimentary Research*, 84(3), 198–214.

Laugier, F.J. & Plink-Björklund, P. (2016) Defining the shelf edge and the three-dimensional shelf edge to slope facies variability in shelf-edge deltas. *Sedimentology*, 63, 1280–1320.

Lazar, O.R., Bohacs, K.M., Macquaker, J.H.S., Schieber, J. & Demko, T.M. (2015) Capturing key attributes of fine-grained sedimentary rocks in outcrops, cores and thin sections: nomenclature and description guidelines. *Journal of Sedimentary Research*, 85(3), 230–246.

Lee, H.J. & Chu, Y.S. (2001) Origin of inner-shelf mud deposit in the southeastern Yellow Sea: Huksan Mud Belt. *Journal of Sedimentary Research*, 71(1), 144–154.

Loucks, R.G. & Ruppel, S.C. (2007) Mississippian Barnett shale: Lithofacies and depositional setting of a deep-water shale-gas

succession in the Fort Worth Basin, Texas. *AAPG Bulletin*, *91*(4), 579–601.

Lowe, D.R. (1982) Sediment gravity flows: II, depositional models with special reference to the deposits of high-density turbidity current. *Journal of Sedimentary Research*, *52*, 279–297.

Macquaker, J.H.S. & Gawthorpe, R.L. (1993) Mudstone lithofacies in the Kimmeridge clay formation, Wessex Basin, southern England: implications for the origin and controls on the distribution of mudstones. *Journal of Sedimentary Research*, *63*, 1129–1143.

Macquaker, J.H.S., Taylor, K.G. & Gawthorpe, R.L. (2007) High-resolution facies analyses of mudstones: implications for paleoenvironmental and sequence stratigraphic interpretations of offshore ancient mud-dominated successions. *Journal of Sedimentary Research*, *77*(4), 324–339.

McCave, I.N., Manighetti, B. & Robinson, S.G. (1995) Sortable silt and fine sediment size/composition slicing: parameters for palaeocurrent speed and palaeoceanography. *Paleoceanography*, *10*(3), 593–610.

Morris, E.A., Hodgson, D.M., Brunt, R.L. & Flint, S.S. (2014a) Origin, evolution and anatomy of silt-prone submarine external levees. *Sedimentology*, *61*, 1734–1763.

Morris, E.A., Hodgson, D.M., Flint, S.S., Brunt, R.L., Butterworth, P.J. & Verhaeghe, J. (2014b) Sedimentology, stratigraphic architecture, and depositional context of submarine frontal-lobe complexes. *Journal of Sedimentary Research*, *84*, 763–780.

Morris, E.A., Hodgson, D.M., Flint, S.S, Brunt, R.L., Luthi, S.M. and Kolenberg, Y. (2016) Integrating outcrop and subsurface data to assess the temporal evolution of a submarine channel–levee system. *AAPG Bulletin*, *100*(11), 1663–1691.

Mulder, T. & Alexander, J. (2001) The physical character of subaqueous sedimentary density flows and their deposits. *Sedimentology*, *48*, 269–299.

Mulder, T., Syvitski, J.P.M., Migeon, S., Faugères, J.C. & Savoye, B. (2003) Marine hyperpycnal flows: initiation, behavior and related deposits. A review. *Marine and Petroleum Geology*, *20*, 861–882.

Mutti, E. & Normark, W.R. (1987) Comparing examples of modern and ancient turbidite systems: problems and concepts. In: *Marine clastic sedimentology*. Dordrecht: Springer, pp. 1–38.

Nardin, T.R., Hein, F.J., Gorsline, D.S. & Edwards, B.D. (1979) A review of mass movement processes, sediment and acoustic characteristics, and contrasts in slope and base-of-slope systems versus canyon-fan basin floor systems. *SEPM Special Publications*, *27*, 61–73.

Newport, S.M., Jerrett, R.M., Taylor, K.G., Hough, E. & Worden, R.H. (2018) Sedimentology and microfacies of a mud-rich slope succession: in the carboniferous Bowland Basin, NW England (UK). *Journal of the Geological Society*, *175*(2), 247–262.

Nittrouer, C.A., Kuehl, S.A., DeMaster, D.J. & Kowsmann, R.O. (1986) The deltaic nature of Amazon shelf sedimentation. *Geological Society of America Bulletin*, *97*(4), 444–458.

Normark, W.R., Hess, G.R., Stow, D.A.V. & Bowen, A.J. (1980) Sediment waves on the Monterey fan levee: a preliminary physical interpretation. *Marine Geology*, *37*, 1–18.

Ogston, A.S., Cacchione, D.A., Sternberg, R.W. & Kineke, G.C. (2000) Observations of storm and river flood-driven sediment transport on the northern California continental shelf. *Continental Shelf Research*, *20*(16), 2141–2162.

Palanques, A., de Madron, X.D., Puig, P., Fabres, J., Guillén, J., Calafat, A., Canals, M., Heussner, S. & Bonnin, J. (2006) Suspended sediment fluxes and transport processes in the Gulf of lions submarine canyons. The role of storms and dense water cascading. *Marine Geology*, *234*(1–4), 43–61.

Patacci, M., Haughton, P.D. & McCaffrey, W.D. (2014) Rheological complexity in sediment gravity flows forced to decelerate against a confining slope, Braux, SE France. *Journal of Sedimentary Research*, *84*(4), 270–277.

Paumard, V., Bourget, J., Payenberg, T., George, A.D., Ainsworth, B.R., Lang, S. & Posamentier, H.W. (2020) Controls on deep-water sand delivery beyond the shelf edge: accommodation, sediment supply, and deltaic process regime. *Journal of Sedimentary Research*, *90*, 104–130.

Pickering, K.T. & Cantalejo, B. (2015) Deep-marine environments of the middle Eocene upper Hecho group, Spanish Pyrenees: introduction. *Earth Science Reviews*, *144*, 1–9.

Piper, D.J.W. (1978) Turbidite muds and silts on deep-sea fans and abyssal plains. In: Stanley, D.J. & Kelling, G. (Eds.) *Sedimentation in submarine canyons, fans, and trenches*. Stroudsburg, Pennsylvania: Dowde Hutchinson & Ross, pp. 163–176.

Pirmez, C., Pratson, L.F. & Steckler, M.S. (1998) Clinoform development by advection-diffusion of suspended sediment: modeling and comparison to natural systems. *Journal of Geophysical Research: Solid Earth*, *103*(B10), 24141–24157.

Plink-Björklund, P. & Steel, R. (2002) Sea-level fall below the shelf edge, without basin-floor fans. *Geology*, *30*(2), 115–118.

Plint, G.A. (2014) Mud dispersal across a cretaceous prodelta: storm-generated, wave-enhanced sediment gravity flows inferred from mudstone microtexture and microfacies. *Sedimentology*, *61*(3), 609–647.

Porębski, S.J. & Steel, R.J. (2003) Shelf-margin deltas: their stratigraphic significance and relation to Deepwater sands. *Earth Science Reviews*, *62*(3–4), 283–326.

Posamentier, H.W. & Kolla, V. (2003) Seismic geomorphology and stratigraphy of depositional elements in deep-water settings. *Journal of Sedimentary Research*, *73*, 367–388.

Posamentier, H.W. and Walker, R. (2006) *Deep-water turbidites and submarine fans*. In: Posamentier H.W. and Walker R. (Eds) Facies models revisited, SEPM, Special Publication 84. Broken Arrow: SEPM Society for Sedimentary Geology, pp. 399–520.

Poyatos-Moré, M., Jones, G.D., Brunt, R.L., Hodgson, D.M., Wild, R.J. & Flint, S.S. (2016) Mud-dominated basin-margin progradation: processes and implications. *Journal of Sedimentary Research*, *86*, 863–878.

Poyatos-Moré, M., Jones, G.D., Brunt, R.L., Tek, D.E., Hodgson, D.M. & Flint, S.S. (2019) Clinoform architecture and along-strike facies variability through an exhumed erosional to accretionary basin margin transition. *Basin Research*, *31*(5), 920–947.

Prather, B.E., O'Byrne, C., Pirmez, C. & Sylvester, Z. (2017) Sediment partitioning, continental slopes and base-of-slope systems. *Basin Research*, *29*(3), 394–416.

Prélat, A. & Hodgson, D.M. (2013) The full range of turbidite bed thickness patterns in submarine lobes: controls and implications. *Journal of the Geological Society, London*, *170*(1), 209–214.

Prélat, A., Hodgson, D.M. & Flint, S.S. (2009) Evolution, architecture and hierarchy of distributary deep-water deposits: a high

resolution outcrop investigation from the Permian Karoo Basin, South Africa. *Sedimentology*, 56(7), 2132–2154.

Puig, P., Ogston, A.S., Mullenbach, B.L., Nittrouer, C.A. & Sternberg, R.W. (2003) Shelf-to-canyon sediment-transport processes on the eel continental margin (northern California). *Marine Geology*, 193(1–2), 129–149.

Pyles, D.R. (2008) Multiscale stratigraphic analysis of a structurally confined submarine fan: carboniferous Ross sandstone, Ireland. *AAPG Bulletin*, 92(5), 557–587.

Pysklywec, R.N. & Mitrovica, J.X. (1999) The role of subduction-induced subsidence in the evolution of the Karoo Basin. *The Journal of Geology*, 107(2), 155–164.

Reading, H.G. & Richards, M. (1994) Turbidite systems in deep-water basin margins classified by grain size and feeder system. *AAPG Bulletin*, 78(5), 792–822.

Schieber, J. (1994) Evidence for high-energy events and shallow-water deposition in the Chattanooga shale, Devonian, Central Tennessee, USA. *Sedimentary Geology*, 93(3–4), 193–208.

Schieber, J. (1999) Distribution and deposition of mudstone facies in the Upper Devonian Sonyea Group of New York. *Journal of Sedimentary Research*, 69(4), 909–925.

Schieber, J., Southard, J.B. & Schimmelmann, A. (2010) Lenticular shale fabrics resulting from intermittent erosion of water-rich muds—interpreting the rock record in the light of recent flume experiments. *Journal of Sedimentary Research*, 80(1), 119–128.

Sinclair, H.D. & Tomasso, M. (2002) Depositional evolution of confined turbidite basins. *Journal of Sedimentary Research*, 72(4), 451–456.

Sixsmith, P.J., Flint, S.S., Wickens, H.D. & Johnson, S.D. (2004) Anatomy and stratigraphic development of a basin floor turbidite system in the Laingsburg formation, Karoo Basin, main Karoo Basin, South Africa. *Journal of Sedimentary Research*, 74, 239–254.

Smith, R.M.H. (1990) A review of stratigraphy and sedimentary environments of the Karoo Basin of South Africa. *Journal of African Earth Sciences*, 16(1–2), 143–169.

Spychala, Y.T., Hodgson, D.M., Flint, S.S. & Mountney, N.P. (2015) Constraining the sedimentology and stratigraphy of submarine intraslope lobe deposits using exhumed examples from the Karoo Basin, South Africa. *Sedimentary Geology*, 322, 67–81.

Spychala, Y.T., Hodgson, D.M., Stevenson, C.J. & Flint, S.S. (2017) Aggradational lobe fringes: the influence of subtle intrabasinal seabed topography on sediment gravity flow processes and lobe stacking patterns. *Sedimentology*, 64, 582–608.

Steel, R.J., Porebski, S.J., Plink-Bjorklund, P., Mellere, D. & Schellpeper, M. (2003) Shelf-edge delta types and their sequence-stratigraphic relationships. In: Roberts, H.H., Rosen, N.C., Fillon, R.H. & Anderson, J.B. (Eds.) *Shelf margin deltas and linked down slope petroleum systems; gulf coast section society of economic palaeontologists and mineralogists, foundation 23rd annual Bob F. Perkins research conference*, Vol. 23. Houston, pp. 205–230.

Stevenson, C.J., Jackson, C.A.L., Hodgson, D.M., Hubbard, S.M. & Eggenhuisen, J.T. (2015) Deep-water sediment bypass. *Journal of Sedimentary Research*, 85(9), 1058–1081.

Steventon, M.J., Jackson, C.A., Hodgson, D.M. & Johnson, H.D. (2020) Lateral variability of shelf-edge and basin-floor deposits, Santos Basin, offshore Brazil. *Journal of Sedimentary Research*, 90(9), 1198–1221.

Stow, D.A.V. & Shanmugam, G. (1980) Sequence of structures in fine-grained turbidites: comparison of recent deep-sea and ancient flysch sediments. *Sedimentary Geology*, 25(1–2), 23–42.

Summerhayes, C.P. (1981) Organic facies of middle cretaceous black shales in deep North Atlantic. *AAPG Bulletin*, 65(11), 2364–2380.

Suter, J.R., Berryhill, H.L. and Penland, S. (1987) Late Quaternary Sea-level fluctuations and depositional sequences, Southwest Louisiana continental shelf. In: *Sea-level and coastal evolution* (Eds D. Nummendal, O.H. Pilkey and J.D. Howard). SEPM Special Publication, 40.

Sweet, M.L., Gaillot, G.T., Jouet, G., Rittenour, T.M., Toucanne, S., Marsset, T. & Blum, M.D. (2019) Sediment routing from shelf to basin floor in the quaternary Golo system of eastern Corsica, France, western Mediterranean Sea. *GSA Bulletin*, 132, 1217–1234.

Sylvester, Z., Deptuck, M.E., Prather, B.E., Pirmez, C. and O'Byrne, C.J. (2012) Seismic stratigraphy of a shelf-edge delta and linked submarine channels in the northeastern Gulf of Mexico. In: Prather B. E., Deptuck M.E., Mohrig D.C., van Hoorn B. and Wynn R.B. (Eds) *Application of the principles of seismic geomorphology to continental-slope and base-of-slope systems: case studies from seafloor and near-seafloor analogues*, SEPM Special Publication 99. Broken Arrow: SEPM Society for Sedimentary Geology, pp. 31–59.

Talling, P.J., Amy, L.A., Wynn, R.B., Peakall, J. & Robinson, M. (2004) Beds comprising debrite sandwiched within co-genetic turbidite: origin and widespread occurrence in distal depositional environments. *Sedimentology*, 51(1), 163–194.

Talling, P.J., Masson, D.G., Sumner, E.J. & Malgesini, G. (2012) Subaqueous sediment density flows: depositional processes and deposit types. *Sedimentology*, 59(7), 1937–2003.

Tankard, A., Welsink, H., Aukes, P., Newton, R. & Stettler, E. (2009) Tectonic evolution of the cape and Karoo basins of South Africa. *Marine and Petroleum Geology*, 26, 1379–1412.

Tankard, A., Welsink, H., Aukes, P., Newton, R. & Stettler, E. (2012) Geodynamic interpretation of the cape and Karoo basins, South Africa. In: Roberts, D.G. & Bally, W. (Eds.) *Phanerozoic passive margins*. Cratonic basins and global tectonic maps: Elsevier, pp. 868–945.

Taylor, A.M. & Goldring, R. (1993) Description and analysis of bioturbation and ichnofabric. *Journal of the Geological Society, London*, 150, 358–368.

Terlaky, V., Rocheleau, J. & Arnott, R.W.C. (2016) Stratal composition and stratigraphic organisation of stratal elements in an ancient deep-marine basin-floor succession, Neoproterozoic Windermere Supergroup, British Columbia, Canada. *Sedimentology*, 63(1), 136–175.

Thiéblemont, A., Hernández-Molina, F.J., Miramontes, E., Raisson, F. & Penven, P. (2019) Contourite depositional systems along the Mozambique channel: the interplay between bottom currents and sedimentary processes. *Deep Sea Research Part I: Oceanographic Research Papers*, 147, 79–99.

Tissot, B., Demaison, G., Masson, P., Delteil, J.R. & Combaz, A. (1980) Paleoenvironment and petroleum potential of middle cretaceous black shales in Atlantic basins. *AAPG Bulletin*, 64(12), 2051–2063.

Trabucho Alexandre, J., Van Gilst, R.I., Rodríguez-López, J.P. & De Boer, P.L. (2011) The sedimentary expression of oceanic anoxic event 1b in the North Atlantic. *Sedimentology*, 58(5), 1217–1246.

Traykovski, P., Geyer, W.R., Irish, J.D. & Lynch, J.F. (2000) The role of wave-induced density-driven fluid mud flows for cross-shelf transport on the Eel River continental shelf. *Continental Shelf Research*, *20*(16), 2113–2140.

Van der Merwe, W.C., Hodgson, D.M. & Flint, S.S. (2009) Widespread syn-sedimentary deformation on a muddy deep-water basin-floor: the Vischkuil formation (Permian), Karoo Basin, South Africa. *Basin Research*, *21*, 389–406.

Van der Merwe, W.C., Flint, S.S. & Hodgson, D.M. (2010) Sequence stratigraphy of an argillaceous, Deepwater basin plain succession: Vischkuil formation (Permian), Karoo Basin, South Africa. *Marine and Petroleum Geology*, *27*, 321–333.

Van der Merwe, W.C., Hodgson, D.M., Brunt, R.L. & Flint, S.S. (2014) Depositional architecture of sand-attached and sand-detached channel-lobe transition zones on an exhumed stepped slope mapped over a 2500 km^2 area. *Geosphere*, *10*, 1076–1093.

Veevers, J.J., Cole, D.I. and Cowan, E.J. (1994) Southern Africa: Karoo Basin and cape Fold Belt. In: Veevers, J.J. and Powell, C.M. (Eds) *Permian-Triassic Pangean basins and foldbelts along the Panthalassan margin of Gondwanaland*, Geological Society America Memoir, 184. Boulder, pp. 223–279.

Viljoen, J.H.A. (1994) Sedimentology of the Collingham formation, Karoo Supergroup. *South African Journal of Geology*, *97*(2), 167–183.

Visser, J.N.J. (1992) Deposition of the early to late Permian Whitehill formation during a sea-level highstand in a juvenile foreland basin. *South African Journal of Geology*, *95*(5–6), 181–193.

Visser, J.N.J. & Prackelt, H.E. (1996) Subduction, mega-shear systems and late Palaeozoic basin development in the African segment of Gondwana. *Geologische Rundschau*, *85*(4), 632–646.

Walsh, J.P. & Nittrouer, C.A. (1999) Observations of sediment flux to the eel continental slope, northern California. *Marine Geology*, *154*(1–4), 55–68.

Wells, J.T. & Coleman, J.M. (1981) Physical processes and fine-grained sediment dynamics, coast of Surinam, South America. *Journal of Sedimentary Research*, *51*(4), 1053–1068.

Wetzel, A. (1984) Bioturbation in deep-sea fine-grained sediments: influence of sediment texture, turbidite frequency and rates of environmental change. *Geological Society, London, Special Publications*, *15*(1), 595–608.

Wright, L.D., Friedrichs, C.T., Kim, S.C. & Scully, M.E. (2001) Effects of ambient currents and waves on gravity-driven sediment transport on continental shelves. *Marine Geology*, *175*(1–4), 25–45.

Wynn, R.B., Masson, D.G., Stow, D.A. & Weaver, P.P. (2000) The northwest African slope apron: a modern analogue for deep-water systems with complex seafloor topography. *Marine and Petroleum Geology*, *17*(2), 253–265.